RSC Sustainability

ROYAL SOCIETY OF CHEMISTRY

CRITICAL REVIEW

View Article Online
View Journal | View Issue

Cite this: *RSC Sustainability*, 2024, **2**, 11

Recent advancements towards the green synthesis of carbon quantum dots as an innovative and eco-friendly solution for metal ion sensing and monitoring

Jyoti Dhariwal, Gyandshwar K. Rao * and Dipti Vaya *

In recent years, the synthesis of carbon quantum dots (CQDs) through green methods for environmental remediation has gained significant interest owing to their benefits of reducing toxic by-products and minimising the usage of hazardous chemicals. CQDs are a new type of zero-dimensional carbon nanomaterials having a size less than 10 nm. They have attracted much attention considering their outstanding optical characteristics, non-toxicity, low-cost synthesis, biocompatibility, uniform particle size, high photostability and highly tuneable photoluminescence. The synthesis of CQDs from biodegradable and renewable resources, such as biowastes and biomass, provides an eco-friendly and sustainable alternative to conventional synthesis methods. The synthesized CQDs possess unique optical and electronic properties, including a high selectivity and sensitivity, making them promising for metal ion sensing. This review highlights the recent progress in the green synthesis of CQDs, including their synthesis methods, optical properties and potential use in sensing applications for the detection of heavy metal ions, such as iron(III), copper(II), mercury(II), chromium(IV), lead(II), silver(I), arsenic(III) and gold(III), which are considered as major environmental pollutants. A comparison based on the quantum yield, sensitivity, selectivity, detection limit, linear range concentration and sensing mechanisms is also presented. In addition, the effect of heteroatom doping on CQD performance for heavy metal detection is also discussed. In conclusion, this review emphasizes the importance of employing eco-friendly and sustainable methodologies for CQD synthesis, which not only benefits the environment but also makes these materials more accessible and cost-effective for widespread use in detecting harmful pollutants.

Received 17th October 2023
Accepted 24th November 2023

DOI: 10.1039/d3su00375b

rsc.li/rscsus

Sustainability spotlight

In an era of increasing environmental concerns and growing awareness towards sustainable synthesis, resource efficiency, waste reduction and minimal environmental impacts have become guiding principles in both the industry and laboratory. These principles guide researchers and industries in developing processes that make use of renewable resources. Researchers are currently exploring novel materials obtained from natural sources, such as plant biomass and agricultural residues, with the aim to replace petrochemical-based precursors. In this review paper, we have covered the green synthesis of carbon quantum dots (CQDs) using natural precursors, focusing on their vital role in the domain of heavy metal ion sensing and monitoring in water, harmonizing scientific progress with ecological responsibility.

Introduction

Carbon-based nano-materials, such as graphene, diamonds, carbon tubes and fullerenes, have attracted much attention from researchers owing to their extraordinary properties. The poor water solubility and weak fluorescence in the visible region limit the application of graphene and fullerenes. Furthermore, the synthesis and separation of nano-diamonds are challenging, thus hindering their applications.[1] Hence, the scientific community explore design and synthesize of new materials that can replace graphene, fullerenes or nano-diamonds, and fluorescent carbon dots are one of these materials. Fluorescent carbon dots include carbon quantum dots (CQDs), carbon nanodots (CNDs) and graphene quantum dots (GQDs).[2] The appearance of CQDs was first ironically noticed by Xu *et al.* in 2004 during the purification of single-walled carbon nanotubes synthesised by an arc-discharge method.[3] CQDs are mono-dispersed quasi-spherical shaped crystalline nano-materials having a size of <10 nm, exhibiting good water solubility, unique optical properties and highly tuneable photoluminescence (PL). CQDs with a surface as large as 60 nm have also been reported.[4] Furthermore, their surface can be easily

Department of Chemistry, Biochemistry and Forensic Science, Amity School of Applied Sciences, Amity University Haryana, Gurugram, Haryana, 122413, India. E-mail: diptivaya08@gmail.com; gyan23iitd@gmail.com; gkrao@ggn.amity.edu

modified without altering their native characteristics. CQDs primarily consist of an amorphous sp^2/sp^3-conjugated carbogenic core with various oxygen/nitrogen-containing groups, such as hydroxyl, carboxyl and amine, on their surface. The composition ratio of surface groups often varies with the carbon precursor used and synthesis routes employed for their synthesis. The presence of surface functional groups on CQDs increases their water solubility, thus providing a greater range of possible applications, mainly in photoelectronic, analytical and biomedical fields.[5] The doping of CQDs with hetero atoms, such as nitrogen, phosphorus and sulphur, can further enhance their properties to a great extent.[6] It has been established that traditional transition metal quantum dots, such as cadmium telluride (CdTe), cadmium sulfide (CdS) and cadmium selenide (CdSe), show better optical characteristics and stability than CQDs. However their costly fabrication and low biocompatibility limit their utility in biomedicines, specifically in theranostic applications.[7] CQDs however show superior biocompatibility, chemical stability, excellent aqueous solubility, high quantum yield (QY), and less toxicity and can be easily synthesised by eco-friendly methods. Such unique properties of CQDs make them more relevant than semiconductor quantum dots (SQDs) and organic dyes for practical applications. Such applications include sensing of metal ions, drug delivery, electrocatalysis, and photocatalysis.[8] Various properties of CQDs are demonstrated in Fig. 1.[9]

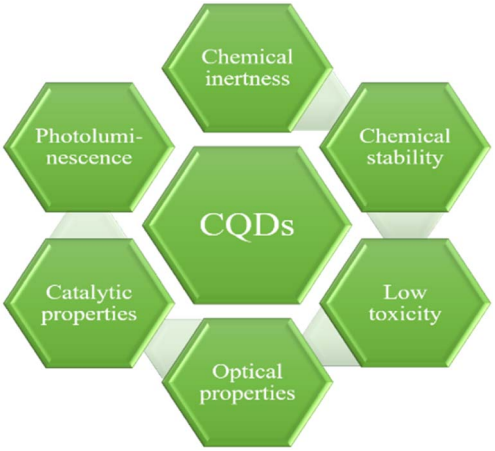

Fig. 1 Properties of CQDs.

Many efforts have been made for developing new, simple, cost-effective and efficient techniques for CQD fabrication with emphasis on non-toxic and environmentally friendly approaches. Biomass has emerged as a sustainable and non-toxic route for the synthesis of highly stable CQDs. Biomass is a large, complex, heterogeneous and biodegradable substance that can be obtained from a variety of sources such as animal

Jyoti Dhariwal

Jyoti Dhariwal, born in Gurugram, Haryana, is currently pursuing her PhD at the Department of Chemistry, Amity School of Applied Science, Amity University Haryana, India, under the supervision of Dr Dipti Vaya. Her research interests include the green synthesis of nanomaterials and their environmental application, specifically sensor application, for heavy metal detection.

Gyandshwar K. Rao

Dr G. K. Rao completed his PhD under the supervision of Professor Akai Kumar Singh at IIT Delhi, India. He worked at the University of Ottawa as a postdoctoral fellow from 2014 to 2017 with Prof. Darrin Richeson. He is currently working as an Assistant Professor at the Department of Chemistry, Amity School of Applied Sciences, Amity University Haryana. His research interests include the design and synthesis of inorganic and organometallic species and nanomaterials for energy and medicine. He co-authored sixty-two research articles published in international journals of high repute and eleven book chapters; he has also edited one book and filed four patents. His H and i-10 index are 28 and 45, respectively.

Dipti Vaya

Dr Dipti Vaya was awarded a PhD degree from MLSU, Rajasthan. She is currently working as an Associate Professor at the Department of Chemistry, Amity School of Applied Science, Amity University Haryana. She has 15 years of teaching and research experience. Her research interests include the development of efficient nanomaterials, polymer nanocomposites, carbon-based materials for waste water treatment and water splitting. She was awarded a DRDO-funded project. She has co-authored various national and international research articles and book chapters. Two scholar PhD degrees have been awarded under her supervision. She has submitted 3 patents. Recently, she is recognized as Top 2% scientists by Stanford University and Elsevier BV. She was also selected as one of the "75 Women in Chemistry in SHE IS", awarded by the Government of India and the Royal Society of Chemistry.

waste, plant parts, algal waste, human sewage and industrial by-products.[10] The main constituents of biomass include hydrogen, carbon, and oxygen, with trace amounts of hetero atoms such as sulphur, nitrogen, phosphorus, and heavy metals ions.[11] Numerous chemical reactions are feasible at biomass due to the presence of various functional groups on the chemical compounds present within them. Nanomaterials derived from biomass shows excellent biocompatibility, nontoxicity, and good water solubility. Even though the formulation of CQDs from natural bio-sources has its own set of obstacles, it is popular due to a number of benefits including pollution-free nature, sustainability, low cost and green preparation processes.[12] Such CQDs have the potential to be used in various applications. Heavy metal ion sensing is one of the most studied applications of these CQDs due to their high QY, low toxicity and good photo stability. CQDs show a strong fluorescence intensity even at very low concentrations. Excellent photostability confirms fluorescence signal stability and thus assuring accurate detection results.[13] CQD-based sensors have shown the selective and sensitive detection of various anions, metal ions and other organic moieties depending on the affinity of different surface groups present on their surface. The limitations of CQDs include their post functionalization, complex purification and separation procedures and structural characterization with respect to their geometries, composition, and crystal shape. Such issues must be addressed before their application in biosensing, nanomedicine and bioimaging.[14] The present review is thus focused on the progress in the field of CQDs with special emphasis on eco-friendly synthesis by hydrothermal, microwave-assisted and carbonisation methods. This also includes the recent development for their utilization as florescent probes for selective detection of different metal ions. Their importance in biomedical, pharmaceutical, and environmental fields is also included.

Synthesis method

Due to the active contribution of several research groups, many simple and cost-effective routes have been developed in order to get the CQDs of desired functionality, size and structure, for specific applications. The synthetic methods of CQDs have been divided into two approaches: "Top-down and Bottom-up". The top-down process involves the synthesis of the CQDs from macroscopic graphite-like structures by breaking them down into nano range either by physical or chemical methods. Several top-down synthesis approaches have been reported and classified into main five categories: (a) chemical oxidation;[15–18] (b) laser ablation;[19] (c) arc-discharge;[3] (d) electrochemical oxidation[20–22] and (e) ultrasonic synthesis.[23] Mono-disperse CQDs with precisely defined molecular structures and sizes are produced using these methods; however, such processes require costly precursors, complex instrumental set-ups and sophisticated facility. Furthermore, the "bottom-up" approach does not require sophisticated techniques and costly precursors, and produces CQDs from cheaper precursors using simple experimental set-ups. This approach involves the synthesis of CQDs using molecular precursors such as carbohydrates, citrate

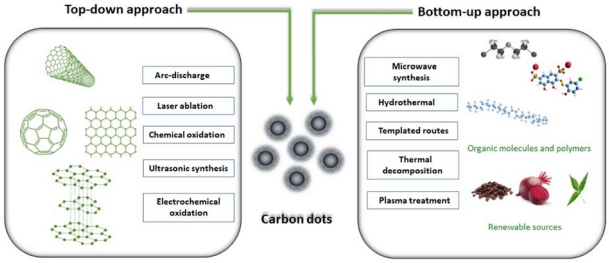

Fig. 2 Synthesis methods of CQDs and their classification.

and polymer–silica nano-composites by either microwave irradiation,[24] thermal decomposition,[25] hydrothermal treatment,[26] template based routes[27] or plasma treatment.[28] The first step in the bottom-up process is to select suitable carbon precursors, which directly influence the characteristics of the resulting CQDs. The second step involves the carbonisation of the selected carbon precursor followed by purification in order to remove impurities that might form during the carbonisation process. This type of CQD synthesis process involves assembling carbon atoms or molecules through chemical processes to form nanoscale carbon structures. Molecules having sufficient functional groups such as hydroxyl/carboxyl are suitable to be used as carbon precursors for this process. A schematic representation of various routes employed for CQD synthesis is summarized in Fig. 2.

The green approaches for the synthesis of CQDs have attracted the attention of scientific community due to their non-venerable nature. Such approach requires a green material as the carbon source for the synthesis of CQDs. The raw materials as well as methods used for the synthesis of CQDs strongly affect the properties including the size, crystallinity, functional groups, colloidal stability, fluorescence properties, QY and compatibility. In the subsequent sections, some representative methods for the green synthesis of CQDs from green carbon precursors are discussed. Mostly hydrothermal, microwave synthesis and carbonisation methods were reported for the fabrication of CQDs using a green carbon source as the raw material. The detailed description of each method is also given.

Microwave synthesis of CQDs

Microwave pyrolysis is considered as one of the best bottom-up techniques for the synthesis of CQDs. It involves breaking off the chemical bonds with the help of high energy microwave radiations.[29] This process requires less time and provides homogeneous heating, resulting in the formation of uniformly sized CQDs. Zhu *et al.* first reported the synthesis of stable luminescence CQDs using microwave.[30] For CQD synthesis, various concentrations of saccharide and polyethylene glycol (PEG-200) were mixed with distilled water to obtain homogeneous solutions. The solutions obtained were then heated in a 500 W microwave oven for 2–10 minutes. A change in solution colour from yellow to dark brown indicates the formation of CQDs. Liu *et al.* have reported the microwave-assisted fabrication of nitrogen-doped carbon quantum dots (N-CQDs) and

CQDs by utilising tomato as the raw carbon source. Nitrogen doping was done with "N" sources such as ethylenediamine and urea. This process generally led to the formation of CQDs along with larger C-nano/-micro particles, which could be removed by centrifugation at a higher speed (rpm) followed by dialysis of the supernatant liquid through a membrane. The solid powder of nanoparticles (NPs) was then obtained by lyophilization.[31] These CQDs were used for the bioimaging of plant pathogenic fungi and the detection of vanillin. A waste cotton linter as the carbon source has been used by Hasan *et al.* for the synthesis of water-dispersed fluorescent CQDs in a very short time *via* a microwave-assisted hydrothermal process. The average particle size of the synthesised CQDs was found to be 10.14 nm.[24] This method is economic and easier than the others reported in the literature; further, the formed CQDs have been used for cancer-imaging applications. In order to check the effectiveness of CQDs in cell imaging, two different concentrations (50 μL mL^{-1} and 100 μL mL^{-1}) of the CQD colloidal solution were applied to a human mesothelioma cell line and human umbilical vein endothelial cells for different durations. However, it was found that the cotton-linter-derived CQDs were cytotoxic to cancer cells and lower their viability, while being cytotoxic to healthy human cells also at the same concentration. Various studies in the literature reported the anti-cancer properties of CQDs, and these properties are largely attributed to the synthesis protocol and carbon precursors used for their synthesis. Lotus root (LR) has also been used as a carbon material for the synthesis of fluorescent N-CQDs showing a high QY of 19%. The CQDs were spherical in shape and their average size was found to be 9.41 nm, as revealed by TEM analysis. These CQDs have been employed for selective mercuric ion (Hg^{2+}) detection and the limit of detection (LOD) was found to be 18.7 nM. The selectivity of LR-CQDs towards Hg^{2+} ions is due to the stronger affinity and quicker chelating kinetics of Hg^{2+} towards hydroxyl, carboxyl and amino groups present on the CQD surface than those of other metal ions. Additionally, the Hg^{2+}/Hg^{+} redox potential is located between the conduction band and the valence band of LR-CQDs, which results in photoinduced electron transfer from the conduction band to the complex states of Hg^{2+} causing quenching of fluorescence intensity. The UV-vis absorption spectra of LR-CDs and LR-CQDs-Hg^{2+} were reported in order to further understand the binding between LR-CDs and Hg^{2+} ions. LR-CQDs show an absorption peak at 280 nm; however, by the addition of Hg^{2+} ions to the LR-CQD solution, the absorption peak significantly diminished, showing the binding of LR-CQDs and Hg^{2+} ions.[32] Zaman *et al.* used fruit bunch biochar for the synthesis of CQDs by a microwave-assisted method. This method gives fluorescent CQDs within few minutes, which have carboxylic, hydroxyl and carbonyl groups at the surface, responsible for their good aqueous solubility. These CQDs were found suitable for the detection of Cu^{2+} ions in their concentration range of 0–400 μM. The plausible reason for fluorescence emission quenching of CQDs in the presence of Cu^{2+} ions is the interaction of CQD surface functional groups with Cu^{2+} ions. The significant fluorescence quenching effect of Cu^{2+} is due to the quick electron transfer between Cu^{2+} ions and oxygen-rich groups on the surface of CQD. These oxygen functional groups on CQD surfaces not only render the water-soluble property, but also exhibit strong interaction with metal ions. The high selectivity of CQDs for Cu^{2+} ions can be explained *via* strong coordination between hydroxyl functional groups on the surface of CQD and Cu^{2+} ions. This interaction enables the transfer of electrons in the excited state of CQDs to the empty 3d orbitals of Cu^{2+} ions, facilitating nonradiative electron/hole recombination that results in a significant reduction in fluorescence intensity.[33] Raw cashew gum has been utilized as the carbon source for aqueous phase synthesis of CQDs in 30–40 min using 800 W microwave radiations. The large particles were then separated by centrifugation. Freeze-drying of the filtrate resulted in a pale brown solid having an average particle size of 9 nm, as revealed by a TEM study.[34] Fluorescent CQDs have been synthesised using lemon and onion juice as carbon precursors (Fig. 3). The size of CQDs was found to be 6.15 nm, which were used for the determination of riboflavin in mineral/multivitamin supplements.[35]

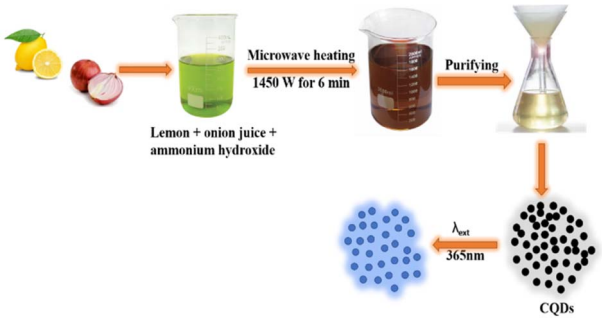

Fig. 3 Synthesis procedure of highly fluorescent CQDs from lemon and onion juices under microwave irradiation.[35]

Hydrothermal synthesis

A hydrothermal technique has been widely used for the synthesis of CQDs using saccharides, organic acids, juices and waste peels. CQDs synthesized by the hydrothermal carbonization process are highly efficient, less expensive, non-toxic, and environmentally friendly with uniform size distribution.[36] The hydrothermal approach involves the heating of the precursor solution (made either in organic solvents or in water) in a hydrothermal reactor having a Teflon tube. At a relatively high temperature and pressure, the organic molecules combined together, resulting in the formation of carbon-seeding cores which further transform into CQDs.[21] Zhu *et al.* synthesized CQDs having very a high QY (about 80%) using a hydrothermal technique.[37] Khan *et al.* used red lentils as the precursor for the synthesis of N-CQDs by a hydrothermal method. The prepared N-CQDs have a QY of 13.2% and exhibit bright blue fluorescence under UV light at an excitation wavelength of 365 nm. These N-CQDs have been used as nano probe sensors for the detection of Fe^{3+} in solutions.[38] Broccoli juice was used for the hydrothermal synthesis of CQDs at 190 °C (Fig. 4). These CQDs showed selective sensing of Ag^{+} ions in aqueous solutions.[39]

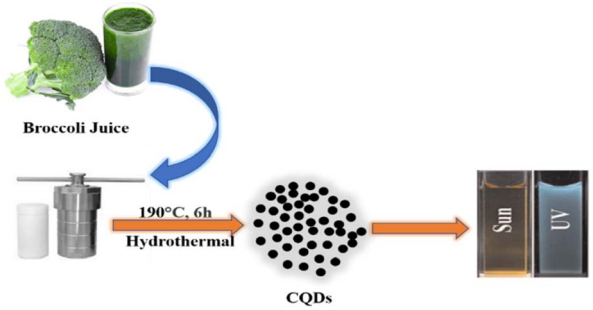

Fig. 4 Synthesis of CQDs from broccoli juice *via* a hydrothermal process.[39]

Fig. 5 A schematic illustration of the synthesis of water-soluble fluorescent CQDs from watermelon peels.[46]

Lu *et al.* reported the synthesis of CQDs *via* a hydrothermal route using pomelo peels as the carbon precursor at 200 °C The resulting solutions were centrifuged to remove unreacted moieties, and the particle size was found to be 2–4 nm. These fluorescence CQDs have a QY of 6.9% and are used for sensing Hg^{2+} ions taken from a lake water sample.[40] Furthermore, banana peel waste has also been utilized as a green source for the synthesis of CQDs *via* a hydrothermal route. Unreacted organic moieties were removed *via* filtration through a mixed cellulose ester membrane. These CQDs have a QY of 20% with an average particle size of 5 nm and appeared bright blue when excited with 365 nm wavelength light. The CQDs have been used for bioimaging in nematodes due to their excellent fluorescence stability and biocompatibility.[26] Yang and co-workers synthesized amino-functionalized fluorescent CQDs by hydrothermal treatment of a chitosan material.[41] Yu *et al.* reported the synthesis of N-CQDs with a QY of 21.9% from *Osmanthus fragrans via* a hydrothermal route. These N-CQDs were employed as fluorescent nano-sensors for Al^{3+} ions.[42] Mehta *et al.* reported the synthesis of blue fluorescent CQDs having a uniform size of ~3.0 nm using sugar cane juice as the source of carbon. The mixture of sugar cane juice and ethanol was heated at 120 °C till a dark brown solution was obtained. Yadav group has reported the synthesis of CQDs using neem as the carbon source. The fluorescence CQDs have a QY of 27.2% and showed peroxidase-like activity towards the oxidation of peroxidase substrate 3,3′,5,5′-tetramethylbenzidine with hydrogen peroxide.[43] Zhang group reported corncob residues (CRs) as carbon precursors for the synthesis of CQDs. Two types of N-CQDs were synthesized using CRs obtained after hemicelluloses pre-extraction and from enzymatically hydrolysed corncob residues (EHCRs). The main components found in CRs are cellulose and lignin, whereas the main component of EHCRs is lignin. The larger particles were removed using a cylindrical filtration membrane filter. Dialysis of the solution was carried out in distilled water using a semi-permeable membrane for 2 days. The final solution was subjected to lyophilization to obtain N-CQDs/E-N-CQDs. These CQDs (average size 9.31 nm) showed adsorption at 270–280 nm, which attributed to the π–π* transition. The E-N-CQDs showed higher fluorescence than that of N-CQDs and are used for the selective detection of Fe^{3+} in blood with an LOD value of 0.75 μmoL L^{-1}. The higher fluorescence of E-N-CQDs than that of N-CQDs is due to the presence of a larger number of aromatic rings associated with the precursor lignin.[44]

Carbonization method

Carbonization is the process of heating materials in the presence/absence of air. The process requires high temperatures. Several green sources have been utilized for the synthesis of CQDs *via* the carbonization process. Highly fluorescent water-dispersible CQDs were prepared by low-temperature carbonization under a nitrogen flow using walnut shells as the carbon precursor. The average particle size was found to be 3.4 nm, as revealed by TEM. These CQDs have been used as bioimaging agents for intracellular trafficking.[45] Watermelon peels, a waste raw resource, were used to prepare CQDs *via* carbonization (Fig. 5). The carbonization process was carried out in air for 2 h at 220 °C and CQDs were obtained by sonication, filtration and centrifugation to remove larger particles. The supernatant liquid having CQDs was dialyzed against distilled water for 48 h to obtain amorphous, blue luminescent spherical shaped, and water-soluble CQDs with an average particle size of 2 nm. These CQDs were efficiently used for live cell imaging, indicating that these carbon NPs can serve as high-performance optical imaging probes.[46] Sun *et al.* described a one-step method for the large-scale synthesis of nitrogen and sulphur-co-doped CQDs (S-N-CQDs) with sulphuric acid carbonization of hair fibers at different temperatures including 40, 100, and 140 °C for 24 hours. The high reaction temperature favoured the formation of high-sulphur content S-N-CQDs of smaller size, which have longer wavelengths of PL emissions. These S-N-CQDs showed good biocompatibility, luminescence stability, low toxicity and high solubility.[47]

Highly fluorescent CQDs have been synthesized by Murugan group using finger millet ragi as the carbon source by a carbonization process at 300 °C. These CQDs have been used as nano sensors for the detection of Cu^{2+} ions in real water samples with an LOD value of 10 nM.[48] Furthermore, fluorescent CQDs having a QY of 19.3% have been synthesized using sweet pepper as the source of carbon. These CQDs have been synthesized *via* a two-step process. The first step involves the low-temperature carbonization of pepper at 180 °C for 5 h and the second step involves the separation of the product. These CQDs have been used as fluorescent probes for hypochlorite

detection in tap water. The LOD value for hypochlorite has been found to be in the order of 0.05 mmoL L^{-1}.[49]

Optical properties of CQDs/ photoluminescence (PL) emissions in CQDs

The absorption of CQDs mainly occurs in the UV region with a tail extending into the visible region. The absorption in the UV region is attributed to the $\pi \rightarrow \pi^*$ transition of aromatic C=C and the $n \rightarrow \pi^*$ transition due to various oxygen- and nitrogen-containing groups present on the CQD surface. For example, CQD synthesis from *Lantana camara* berries shows two peaks in the UV region: one at 285 nm attributed to the $\pi \rightarrow \pi^*$ transitions of C=C and the other peak at 356 nm attributed to the $n \rightarrow \pi^*$ transition (Fig. 6). The aqueous CQD solution shows a pale yellow colour under day light and illuminates bright blue colour under UV light.[50]

Fluorescence is one of the most studied properties of CQDs from both practical application and fundamental study point of view. Although the fluorescence of CQDs has attracted huge attention, the exact mechanism of fluorescence in CQDs is still a topic of discussion. Various theoretical mechanisms have been proposed for the occurrence of PL in CQDs, which lack experimental evidence. It has been suggested that the PL in such CQDs might have different excitation, which results in dependent emission, probably due to their wide size range, distinct surface defects/states, availability of different surface groups or varying degree of π-conjugation. The PL phenomenon in CQDs arises either due to their size or due to surface defects.[51] Size-dependent PL emission in CQDs is one of the most fascinating properties of these materials.[52] Smaller size of quantum dots results in a larger band gap and *vice versa*.[53] The synthetic procedure has a significant effect on the PL of CQDs as it controls the size and defects.[54] Kang and co-workers synthesized CQDs having blue, green, yellow, and orange emissions respectively under similar energies of excitation, which attributed to their size difference. These CQDs were treated with H_2 to remove surface oxygen species; however, no significant change in the PL spectra was observed. Hence, it could be concluded that oxygen molecules present either on the CQD surface or in solutions are not responsible for luminescence, rather it is due to their smaller size.[55] The red shift in the emission wavelength of CQDs with the increase in size was reported by Mohapatra *et al.*[56] Nevertheless, various surface defects on the surface of CQDs can also govern the PL, which is due to the presence of various functional groups rather than their size. Thus, the PL of CQDs is affected by the size as well as the presence of surface defects. It has also been reported that the PL of CQDs might also be controlled by functional groups in a synergistic manner.[37] Bao *et al.* reported the synthesis of CQDs of varying sizes by an electrochemical method using carbon fibres at different potentials. It has been observed as the sizes of CQDs decreased, the emission peak shifted to a lower energy state at identical excitation wavelengths. This phenomenon is not in accordance with the "Quantum-Confinement Effect". The smaller sized CQDs were formed at higher potentials and are more oxidized, hence they bear more oxygen-containing groups on the surface. Therefore, the red shift in the emission spectra of CQDs is due to the change in surface states rather than the size effect. Similarly, the acid-treated CQDs did not show observable PL properties until their surface has been modified by amine-containing polymers. The presence of surface energy traps that become emissive upon stabilisation as a result of surface passivation may explain the PL from CQDs. A study conducted by Sun and his co-workers reported the synthesis of CQDs by laser ablation of a carbon target in the presence of water vapor with argon used as a carrier. According to electron microscopy investigations, the as-produced samples have abundance of nanoscale carbon particles arranged in clusters of varying sizes. However, no detectable PL was observed from either sample or its aqueous suspension. The sample was then further treated with a 2.6 M aqueous nitric acid solution, but still there is no significant PL. Bright luminescence emissions were found after surface passivation by attaching simple organic molecules to acid-treated carbon particles. Various organic molecules including poly(propionylethylene-imine-*co*-ethyleneimine) and diamine-terminated oligomeric poly(ethylene glycol) could serve as surface passivating agents. After passivation with organic moieties, the CQDs show strong PL in both solid state and solution-like suspension. The resulting emission covers a wide range of visible wavelengths that also extended into near-infrared wavelength ranges. It seems that CQDs require surface passivation to exhibit PL, and the widely accepted mechanism for the explanation of luminescence emission in CQDs is radiative recombination of excitons.[19] The CQD sample with similar sizes but different degrees of surface oxidation have been reported and found to show emission from 440 to 625 nm. The plausible red shift can be explained in terms of decrease in band-gap due to the increase in the number of oxygen-containing functional groups on the CQD surfaces.[57] Deng *et al.* reported excitation wavelength-independent fluorescence emission of the CQDs, having a size range between 4 and 10 nm and identical surface-branched polyethyleneimine. The difference in the fluorescence emission is mainly attributed to the

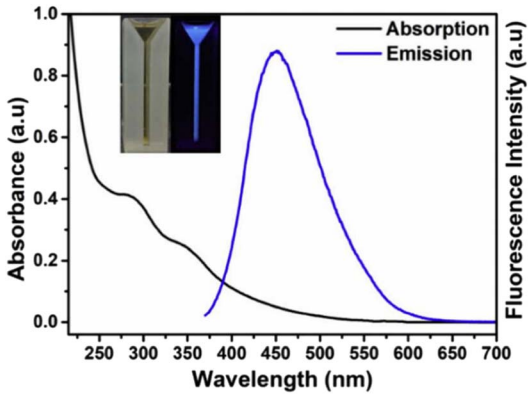

Fig. 6 UV-vis spectra of CQDs synthesized from *Lantana camara* berries. Reproduced from ref. 50 with permission by Elsevier, copyright 2023.

size of CQDs.[58] Giannelis and co-workers carried out temperature-controlled carbonisation using ethanolamine and citric acid at different temperatures for the synthesis of CQDs. The CQDs having a high QY of 50% were obtained at low temperatures and PL is mainly due to the presence of amide-containing organic fluorophores. At a higher temperature, pyrolysis results in the formation of spherical shaped particles with an average diameter of 19 nm and their QY has been decreased to 15%. The decrease in the QY is due to the fact that the pyrolysis at higher temperatures results in the utilization of organic fluorophores for the formation of carbogenic cores.[59] Recent studies have reported a new and intriguing phenomenon of fluorescence known as up-conversion fluorescence emission. It is defined as the longer excitation wavelength produces the shorter emission wavelength. Absorbing numerous infrared photons and releasing one visible photon is a typical example of this type of fluorescence. Three components have been reported to contribute to up-conversion fluorescence; (a) photon avalanche, (b) excited-state absorption and (c) energy transfer up-conversion. The measure of the excitation intensity-dependence fluorescence is a conventional method in order to differentiate up-conversion fluorescence from regular originated fluorescence.[60] The up-conversion PL of N-CQDs in the wavelength range of 750–960 nm has been reported by Sutiman.[61] Lin showed that the CQDs emitted strong up-conversion fluorescence with an excitation wavelength of 800 nm, which is due to two-photon excitation.[62] The up-conversion fluorescence can be easily observed with naked eyes.[63]

Mechanisms of heavy metal detection using CQD-based sensors

Although several theories have been outlined to describe the mechanism of metal ion sensing by CQDs, the exact mechanism is still a subject of debate among the scientific community.[64] Some basic sensing mechanisms include fluorescence resonance energy transfer (FRET), coordination-induced aggregation, inner filter effect (IFE), FL quenching, photo-induced electron transfer (PET) and ion binding/aggregation. The optical absorption properties of CQDs are mainly responsible for their use in designing optical sensors for heavy metal detection. The optical absorption properties occur from the photo-excitation of charge carriers in CQDs and the subsequent transfer of electrons from the valence band to the conduction band. The generated electron–hole species are then used for metal ion sensing based on the particular interactions between metal ions and the surface functional groups of CQDs.[65] Most of the CQD-based sensors work on the principle of either quenching or attenuation of the CQD fluorescence emission in the presence of the analyte, which might be some other species or a metal ion itself.[66] The CQDs show maximum fluorescence in aqueous solutions, but due to the presence of a quencher in the solution, the fluorescence emission intensity gets diminished. The fluorescence emission of the CQDs has been reported to depend on the functional groups present on the surface. The oxygen moieties or other functional group present on the CQD surface selectively coordinate with heavy metal ions causing a change in fluorophore properties such as anisotropy, fluorescence intensity and lifetime. This results in a signal than can indicate analytes with high sensitivity and selectively as a result of quantum confinement. Such changes might be attributed to the energy transfer between the probes and metal ions *via* selective interactions. All these features such as edge structures, surface functionalities, size and morphology of CQDs have an impact on selectivity.[51] Some of the metal ion sensing mechanisms are given below.

Complex formation

One of the most accepted mechanisms for the detection of metal ions using CQDs is complex formation. FTIR spectroscopy is widely used for the detection of various oxygen-containing functional groups such as –COOH, –OR, C=O, and –OH on the CQD surface. Further, surface modification can also be done by doping with hetero atoms such as phosphorus, nitrogen and sulphur to add other groups such as –CN, $–NO_2$, $–NH_2$, $–SO_3H$ and –SH on the surface.[64] It is reported that the metal ion sensing property of CQDs gets enhanced by doping with electronegative atoms. These groups form a coordination complex with metal ions by donating their lone pair of electrons. For example, the Au^+ ion sensing has been carried out using CQDs synthesized from peach gum and jackfruit seeds. The presence of nitrogen donor functional groups on the CQD surface is responsible for their sensing properties, as revealed by spectroscopic measurements. The solution of CQDs showed a change in colour from light blue to dark blue under UV-light after the addition of Au^+ ions, and the LOD value was found to be 0.064 μM.[67,68] The PL property of CQDs is also affected by the nature of the functional group present on the surface, as these groups govern their hydrogen bonding capacity, which, in turn, affects their optical property. CQD surface functional groups can serve as electron-withdrawing and electron-donating groups, and thus can change the CQD surface charge. This surface charge influences the CQDs' ability to establish hydrogen bonds with other molecules, which can cause changes in the energy levels of the excitons responsible for the PL effect. The CQDs synthesised by using D-glucose and sago waste have been utilised as selective fluorescence detectors for lead (Pb^{2+}) ions, and a decrease in the fluorescence emission intensity was observed due to Pb^{2+} ion complexation on the CQD surface. The interaction of metal ions with functional groups such as –OH, C=O and –COOH on the surface of these CQDs can be concluded using FTIR data.[69,70] Bi *et al.* reported the fluorescence emission quenching of CQDs synthesized using turbot fish in the presence of Fe^{3+} ions. The IR data confirm the presence of $–NH_2$ and –OH groups on the CQD surface, and their interaction with Fe^{3+} ions would result in the quenching of fluorescence emissions.[71] A hydrothermal method has been used to synthesize N-CQDs from red lentils and utilized for the selective detection of Fe^{3+} ions. The presence of amide and hydroxyl groups on the surface of CQDs was confirmed by FTIR analysis, which might be due to the presence of proteins and

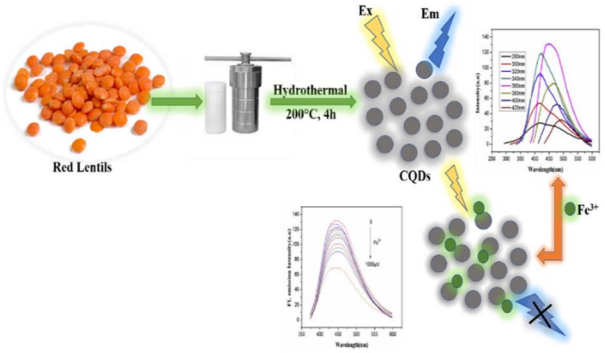

Fig. 7 Synthesis of CQDs using red lentils for Fe^{3+} ion detection.[38]

carbohydrates in red lentils. The addition of Fe^{3+} to the solution of N-CQDs results in a reduction in fluorescence emission intensity probably due to the interaction of amide/hydroxyl functionalities with Fe^{3+} ions (Fig. 7).[38]

N-CQDs synthesized using chitosan have also been reported as a detection probes for Hg^{2+} ions with an LOD of 80 mM. These N-CQDs showed a maximum fluorescence intensity at 440 nm, and the addition of Hg^{2+} ions resulted in a reduction in fluorescence intensity. The fluorescence decay showed a linear behaviour with a Hg^{2+} concentration within the range of 80–300 μM. The linear range of detection in case of CQD metal ion sensing involves the concentration range of metal ions in solutions that can be precisely quantified and detected by CQDs.[72] Sachdev and co-workers reported a hydrothermal method for the synthesis of CQDs using coriander leaves and used them for the detection of Fe^{3+} ions. FTIR data showed the presence of carboxyl groups on the CQD surface, which produce carboxylate ions. These groups interact with Fe^{3+} ions, resulting in the quenching of fluorescence emissions of 400 nm, which is evident from the FTIR studies.[73] CQDs have been synthesized using bamboo leaves and then modified with branched polyethyleneimine. These CQDs have been utilised as sensitive and selective fluorometric sensors for Cu^{2+} ions having an LOD value of 115 nM. FTIR and XPS data conclude the formation of cupric–amine complexes responsible for fluorescence emission

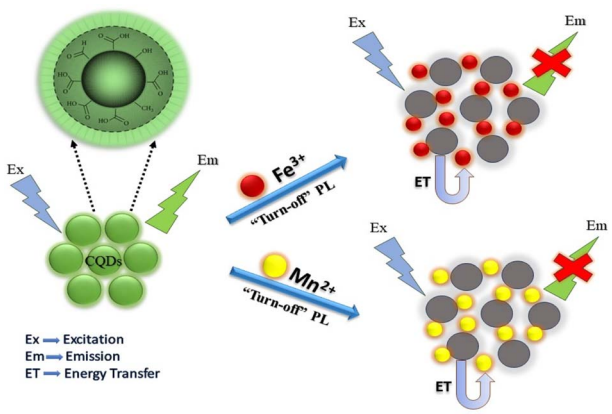

Fig. 8 Quenching mechanism of the synthesised CQDs for Mn^{2+} and Fe^{3+} ions.[75]

quenching.[74] Krishnaiah *et al.* reported the green synthesis of CQDs utilising waste biomass of *Poa parentis* for Mn^{2+} and Fe^{3+} ion sensing. The possible sensing mechanism of CQDs towards these ions is due to the formation of complexes between metal cations and negatively charged surface CQDs. This complex formation results in charge transfer between CQDs and metal ions due to non-radiative recombinations, leading to a decrease in fluorescence intensity.[75] The graphical representation of the quenching mechanism is shown in Fig. 8.

Inner filter effect (IFE)

IFE is also known as apparent quenching, which is an important fluorometric non-radiative energy transfer process that occurs *via* the overlapping of quencher's absorption spectrum with the CQD excitation or emission spectra. It is not a quenching process but it is rather due to the attenuation of the excitation wavelength or absorption of emitted or excited wavelengths by an extra content of chromophoric or fluorophoric species or due to the presence of some other absorbing species in the detection medium.[76] Despite the fact that this effect leads to a reduction in intensity with no time decay, it could not be entitled as quenching. This is a process in which a second absorber declines the particle emission. The IFE effect can be still observed if the separation between re-absorber and emitter is more than ten nano meters.[77] In this process, the absorption peaks of the CQDs were not affected, suggesting that no new complexes were formed, thus the fluorescence lifetime of CQDs was not affected. To understand the IFE mechanism of CQDs, sophisticated instruments are not required, thus it is less expensive and easy to operate. The metal ion concentration does not affect the life time of fluorescence quenching in IFE. This mechanism was investigated for the detection of Cr(VI) using CQDs as sensors. It was found that the absorption bands of Cr(VI) were completely overlapped with the excitation and emission spectra of CQDs.[78] The fluorescence emission quenching of CQDs synthesised using pineapple in the presence of Fe^{3+} has also been found to follow IEF.[79]

FRET mechanism

FRET is an electro dynamic phenomenon, which primarily relies on energy transfer from donors (CQDs in present case) in the excited state to the quencher (also known as acceptor) in its ground state due to the overlapping of the donor emission spectrum with the absorption spectrum of the quencher. The energy transfer efficiency (E) can be derived according to eqn (1).[77] The amount of energy transferred typically depends on four factors: (i) the extent of spectral overlap between the donor emission and the acceptor absorption, (ii) the donor unit's fluorescence QY, (iii) the relative geometric orientation of the donor and acceptor units, transition dipoles and (iv) the relative distance between the donor and acceptor molecules.[80] The sensors showing FRET mechanism generally have low LOD values and high accuracy. FRET occurs without any photon appearance due to long-range dipole–dipole interactions between CQDs and the quencher. The CQD and quencher distance should be in the range of 10–100 Å. The Förster

distance (R_0) between the quencher and CQDs and the CQD-quencher distance (r) can be calculated using eqn (2)–(4).[81,82] CQDs-FRET-based sensors have several advantages over organic dyes and fluorescent protein FRET-based sensors. These include high molar extinction coefficients, excellent photostability, broad absorption spectra, symmetric and narrow emission spectra in the infrared to ultraviolet range, high QYs, good aqueous solubility and extended fluorescence lifetimes.[83] CQDs showing FRET mechanisms can sense both inorganic and organic analytes. Common examples of inorganic analytes include Co^{2+}, Cu^{2+}, $Fe^{3+/2+}$, sulfide ions, and ammonia. Shen *et al.* reported FRET in CQDs synthesized using sweet potato hydrothermally in the presence of Fe^{3+} ions with an LOD value of 0.32 μM:[84]

$$E = 1 - \tau/\tau \quad (1)$$

$$R_0 = 0.211[\kappa^2 n^{-4} \Phi J(\lambda)]^{1/6} \text{ [in Å unit]} \quad (2)$$

$$E = 1/\{1 + (r/R_0)^6\} \text{ [in Å unit]} \quad (3)$$

$$\int_0^\infty F_D(\lambda)\varepsilon_A(\lambda)^4 d \quad (4)$$

τ and τ_0 are the lifetimes in the absence and presence of quencher respectively. κ: orientation factor of CQDs and the quencher transition dipoles and taken as 2/3. Φ: QY of the CQDs. n: refractive index of medium. $J(\lambda)$: integral of overlap values. $F_D(\lambda)$: corrected fluorescence intensity of the CQDs. $\varepsilon_A(\lambda)$: Quencher's extinction coefficient.

Ion binding

Different kinds of functional groups could arise on the surface of quantum dots depending on their synthetic protocol and precursors used. Every functional group has a specific affinity towards a particular metal ion.[85] This is why CQDs synthesized using different precursor/synthetic protocols showed selectivity towards different metal ions. For example, N-CQDs showed selective sensing ability towards Cu^{2+} ions due to the presence of nitrogen atoms on their surface. Although FT-IR and XPS data suggest the presence of –OH, –COOH, and C=O groups, Cu^{2+} only binds to $-NH_2$ groups to form a copper–amine complex. The appearance of a new IR absorption band at 256 nm attributed to the formation of a copper–amine complex.[86]

Aggregation

Aggregation-caused fluorescence quenching is a phenomenon in which a fluorophore molecule displays strong luminescence in dilute solutions, but in concentrated solutions or in solid state the fluorescence intensity is decreased or sometimes even disappears completely. A majority of CQDs because of their reabsorption and quenching effects at high concentrations show this phenomenon. As a result, above a certain (low) concentration, the PL intensity of CQDs decreases as the concentration increases. At high concentrations, small organic luminescent molecules are close enough, as their planar polycyclic aromatic structure enables them to orientate due to strong intermolecular π–π stacking interactions. This superposition of organic molecules allows the photoexcited state to return back to the ground state *via* the nonradiative transition, resulting in fluorescence quenching. CQDs are also composed of similar planar aromatic ring structures, thus it can be assumed that a similar quenching process occurs as the concentration of CQDs increases. The aggregation phenomenon can be prevented *via* molecular conformation control or by incorporating bulky groups such as bulky rings.[87] The instability of CQDs followed by their interaction with the metal ions has been reported to cause precipitation or aggregations. Ansi *et al.* reported the aggregation of CQDs synthesized using table sugar with Pb^{2+} ions, which results in a visual change. The clear brown solution of CQDs becomes off-white due to aggregation after the addition of Pb^{2+} ions.[88] TEM, XRD and EDAX studies revealed the aggregation facts. Furthermore, N-CQDs synthesized using jackfruit result in aggregation after the addition of Au^+ ions, which results in the quenching of N-CQD fluorescence.[89]

PET quenching mechanism of CQDs

Photo-induced electron transfer (PET) is an oxidation–reduction process involving electron transfer from one system to another. In case of CQDs, the PET can occur from CQDs to metal ions or *vice versa*, resulting in the formation of cations and anions respectively. This process involves the formation of complexes in excited state, which returns to a lower energy state without emission of a photon.[90] The emission intensity is generally quenched by the analyte *via* ion coordination. The nature of PET could be reductive or oxidative. In reductive PET, CQDs can act as electron receptors and can receive electrons from the donor molecules. Oxidative PET is the polar opposite of reductive PET. The energy gap between the LUMO of quenchers and the HOMO of CQDs governs the reductive electron transfer. In oxidative electron transfer, the energy gap between the LUMO of the CQDs and the LUMO of the quencher controls the process.[77,91,92] CQDs can detect both inorganic and organic species, which operate through PET mechanism. CQDs having surface carboxyl groups have been reported to selectively sense Cu^{2+} ions, resulting in CQD fluorescence quenching, and follow the PET mechanism.[93] Song *et al.* have observed the fluorescence quenching of CQDs in the presence of Fe^{3+} ions, which is attributed to the non-radiative transfer of electrons from the excited state of sensors to the d-orbital of receptors.[94] A

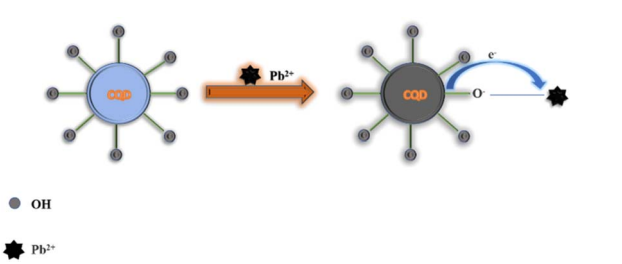

Fig. 9 Synthesis of CQDs using chocolate and their fluorescence quenching after the addition of Pb^{2+} ions following PET.[97]

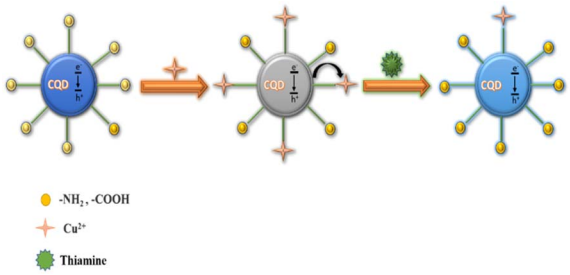

Fig. 10 Fluorescence quenching of CQDs by Cu^{2+} following the PET mechanism and the recovery of fluorescence after adding thiamine.[98]

similar mechanism has been reported for CQDs (synthesized from tea) and Fe^{3+}.[95] A similar mechanism of electron transfer from the excited state of CQDs to the LUMO of Hg^{2+} has been proposed by Vandaukhuzhali *et al.* These CQDs have been hydrothermally synthesized using pineapple.[96] Liu *et al.* synthesized CQDs using chocolate by a hydrothermal method.[97] The fluorescence intensity of these CQDs has been quenched by Pb^{2+} ions, which followed the PET quenching mechanism, as given in Fig. 9. Purbia *et al.* prepared CQDs using tender coconut water *via* a microwave-assisted hydrothermal technique.[98] This CQD fluorescence intensity has been quenched in the presence of Cu^{2+}, which followed the PET quenching mechanism (Fig. 10). The fluorescence intensity of these CQDs was further recovered by the addition of thiamine. CQDs prepared from pipe tobacco exhibited a decrease in fluorescence intensity upon addition of Cu^{2+} ions with an LOD value of 0.01 μM, respectively. The photo-induced transfer of electrons from the excited state of CQDs to the d-orbital of Cu^{2+} is responsible for the fluorescence quenching of these CQDs.[99]

Heavy metal ion sensing using CQDs

Heavy metals including iron, chromium, copper, and aluminium are nutritionally essential elements needed by various organisms to sustain their lives. These elements have a density higher than that of water, and are the most common toxic and non-biodegradable contaminants. Their increased employment in various fields led to an increase in environment pollution. In order to identify the presence of heavy metals and to prevent their negative consequences, the development of eco-friendly, feasible and efficient sensors is required. Due to the unique physiochemical properties of SQDs and their ligand binding tendency, versatile surface chemistry and capability of attachment to various functional materials, SQDs were potentially utilised for the fabrication of sensitive fluorescence sensors during the last decade.[100] Nevertheless, the high fabrication cost and toxic effects of conventional SQDs make them unsuitable for their use as detection systems. However, CQDs which are generally synthesised from natural precursors possess low cytotoxicity and chemical inertness, and their surface can be easily modified due to the presence of various functional groups. Furthermore, the oxygen-containing groups present on the CQD surface are capable of interacting with metal ions and can be efficiently used as sensors. A wide range of CQD-based sensors for the detection of toxic metal ions such as lead, chromium, iron, aluminium, arsenic, cobalt, cadmium, copper, gold, silver and mercury have been reported and will be discussed in the following sections.

Ferric ion detection

Iron is one of the most crucial metal ions in biological systems and is present mainly in two oxidation states, *i.e.*, ferric(III) and ferrous(II).[101] Among these states, the ferric state is more toxic due to its insolubility and causes formation of hazardous radicals. The abnormal presence of Fe^{3+} can results in many serious diseases including anaemia, heart failure, mental decline, and diabetes. The maximal acceptable limit of Fe(III) in drinking water is 5.36 mM according to World Health Organization standards.[102] Therefore, it becomes essential to monitor the Fe^{3+} ion concentration present in the environment and also in biological systems. CQDs have emerged as efficient materials for this purpose due to the presence of various functional groups such as hydroxyl, amino and carboxyl on their surface, which efficiently bind with Fe^{3+} and can lead to fluorescence quenching. These CQDs have been synthesised using different carbon precursors possessing different binding properties due to the different composition of surface functional groups, and thus, they exhibit different sensitivities and selectivities. For example, Architha *et al.* reported the synthesis of spherical shaped, blue-emitting CQDs from a Mexican mint extract and utilized them for Fe^{3+} ion detection. The size of these CQDs was found to be 2.43 ± 0.02 nm with an LOD value of 0.53 μM and a linear concentration range of 0–15 μM. The CQD solution showed a maximum emission intensity at 447 nm, which gets decreased by the addition of different metal ions. The requenching of CQD fluorescence spectra was obtained by adding ascorbic acid to the CQD-metal solution. It was reported that ascorbic acid and Fe^{3+} have a high binding affinity, and the

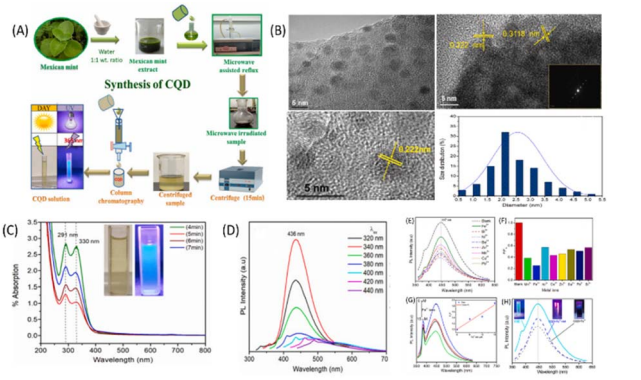

Fig. 11 (A) Synthesis of CQDs. (B) TEM spectra of the synthesized CQDs. (C) UV-vis spectra of CQDs. (D) PL spectra of blank CQDs. (E) PL spectra of CQDs in the presence of different metal ions. (F) Difference in the relative PL intensities of CQDs between the blank and solutions containing different metal ions. (G) CQD PL spectra in the presence of varying Fe^{3+} ion concentrations; the inset shows the linear relationship between F_0/F and the concentration of Fe^{3+} in the range of 0–15 μM. (H) PL spectra of fluorescence quenching and re-quenching properties. Reproduced from ref. 103 with permission by Elsevier, copyright 2023.

fluorescence restoration of CQDs is attributed to the release of loosely bound Fe^{3+} ions from the CQD surface by adding 15 μM ascorbic acid solution. To prove this mechanism, a turn ON–OFF assay was performed, and the logic gate operation was also studied. The graphical representation of the synthesis of CQDs and their characterisation using a Mexican mint extract is shown in Fig. 11. The maximum decrease was observed for Fe^{3+} ions and the minimum decrease for Ni^{2+} ions. Thus, this showed high selectivity for Fe^{3+} ions. The Fe^{3+} ion selectivity with CQDs is attributed to the presence of oxygen groups on the CQD surface, which binds with Fe^{3+}. The complex formation results in a change in the distribution of surface energy traps and enhancement of the non-radiative recombination of electrons and holes, which leads to fluorescence quenching.[103] Edison *et al.* reported the green synthesis of N-CQDs by hydrothermal carbonization of a *Prunus avium* fruit extract, which have a QY of 13%. The synthesized N-CQDs showed maximum fluorescence emission intensity at 411 nm, which gets quenched by adding Fe^{3+} ions due to the formation of a stable complex. The presence of phenolic hydroxyl groups was confirmed by FT-IR and XPS spectroscopy data. The sensing of Fe^{3+} ions has been carried out in water, and the LOD values were found to be 0.96 μM with a linear range from 0 to 100 μM. A wide linear range of detection indicates that the sensing system can accurately detect and quantify a wider concentration range of metal ions. The mechanism for fluorescence quenching has been reported to be non-radiative electron or energy transfer from the N-CQD surface to the metal. The facile synthesis of highly luminescent CQDs using *Prunus cerasifera* fruits has also been reported. The aqueous solution of CQDs shows bright blue fluorescence. The fluorescence intensity of CQDs was selectively quenched by Fe^{3+} ions in the concentration range of 0–0.5 mM.[104] Recent studies have reported that doping of CQDs with hetero-atoms other than nitrogen results in improved sensitivity and selectivity towards Fe^{3+} ions. Wu *et al.* reported a straight forward hydrothermal strategy for the fabrication of blue-emissive sulfur-doped CQDs with an average size of 3.2 nm and a QY of 4.4% using Vitamin B1 in the presence of ethylenediamine. These CQDs have been used as novel fluorescent sensors for the sensitive and selective detection of Fe^{3+}. The LOD value obtained for Fe^{3+} was 177 nM.[105] Aslandaş *et al.* reported the green synthesis of CQDs by sonication of blueberries and used them as sensors for Fe^{3+} detection in the concentration range of 12.5–100 μM. The sensitivity of the CQDs was examined by screening various metal ions such as Pb^{2+}, Hg^{2+}, Mn^{2+}, Ag^{+}, Zn^{2+}, Cd^{2+}, Cr^{3+}, Cu^{2+}, Fe^{3+}, Na^{+} and Pb^{2+}. It has been observed that the fluorescence intensity of these CQDs gets maximum quenched in the presence of Fe^{3+} ions, while other metal ions show a small decrease in fluorescence intensity. The formation of CQD–Fe^{3+} complexes seems to prevent the radiative recombination of excitons and promotes charge transfer, thus resulting in fluorescence quenching. The temperature-dependent fluorescence and absorption measurements were also studied and it was found that there are very less changes in the absorption spectrum by increasing the temperature. Furthermore, the fluorescence intensity decreases gradually with the increase in temperature as the non-radiative transitions get enhanced with the temperature.[106] Lu *et al.* reported the synthesis of N-CQDs *via* hydrothermal carbonization of watermelon juice and CQDs have a QY of 10.6%. The fluorescence emission of N-CQDs was potentially quenched by Fe^{3+} ions, while other metal ions show negligible fluorescence quenching. The high selectivity towards Fe^{3+} ions was attributed to the interaction between surface functional groups, *i.e.*, carboxyl hydroxyl and amine groups of N-CQDs with Fe^{3+} ions. The LOD value was found to be 0.16 μM.[107] Liu *et al.* reported a simple, green, and low-cost method for CQD synthesis *via* hydrothermal treatment of rose-heart radish. These CQDs have a fluorescent QY of 13.6% and utilised for the facile detection of Fe^{3+} in the linear range from 0.02 to 40 M with an LOD value of 0.13 M.[108] Yang *et al.* reported the fabrication of CQDs using mangosteen pulp by a calcination method These CQDs showed strong blue fluorescence under ultraviolet illumination. The fluorescence has been quenched in the presence of Fe^{3+} ions, resulting in the formation of CQDs/Fe^{3+} complexes. The LOD value was found to be 52 nM.[109] Venkatesan *et al.* used the *Boswellia ovalifoliolata* bark extract for the synthesis of water-soluble CQDs with size 4.16 ± 0.22 nm and used them for Fe^{3+} detection. These CQDs showed strong green emissions under UV light and have a QY of 10.2%. They have been used as sensitive and selective probes for Fe^{3+} ions with a linear relationship up to the concentration of 500 μM and an LOD value of 0.41 μM has been observed.[110]

Copper ion detection

Copper (Cu^{2+}) ions are commonly present in human body and involved in various biological processes. However, the long-term exposure to these ions can result in a number of diseases including liver damage, urinary stone, Parkinson's and Alzheimer's diseases.[111] Similar to Fe^{3+} ion detection by CQD-based sensors, several studies have been reported for the fabrication of reusable and steady sensors with high selectivity and sensitivity for Cu^{2+} ions. Chaudhary *et al.* reported the synthesis of spherical shaped, fluorescent N,S-doped CQDs using banana juice as the carbon source by a hydrothermal method. The average size of CQDs was found to be 1.27 nm with a QY of 32%. These N,S-CQDs were further utilized as novel florescent probes for the detection of Cu^{2+} in the water sample with LOD values of 0.3 μg mL^{-1}. The decrease in the fluorescence intensity after the addition of Cu^{2+} ions has been observed and found to be linear from 1 to 800 μg mL^{-1}. The reason for this quenching is the formation of complexes between functional groups present on the CQD surface and Cu^{2+} ions along with charge transfer between N,S-CQDs and Cu^{2+}, which showed non-radiative recombination.[112] In another study, Murugan and co-workers used finger millet ragi for the synthesis of fluorescent CQDs having a size in the range from 3 to 8 nm. These CQDs sense Cu^{2+} ions in real water samples at a very low Cu^{2+} ion concentration of 10 nM. A linear correlation has been observed between the quenching efficiency and the concentration of Cu^{2+} ions in the range from 0 to 100 μM.[48] Tai reported the synthesis of florescent CQDs from human fingernails having an average size of 1.72–5.85 nm and used them for Cu^{2+}

detection. These CQDs selectively detect Cu^{2+} at a much low concentration of 1 nM. XPS and FTIR studies suggest the complex formation with Cu^{2+} and carboxylate/amino groups present on the CQD surface. A linear correlation was obtained between the quenching intensity and the concentration of Cu^{2+} ions in the linear range of 0–1 nM.[113] Qu and co-worker reported the conjugation of *N*-(2-aminoethyl)-*N*,*N*,*N*′-tris(pyridin-2-ylmethyl)ethane-1,2-diamine (AE-TPEA) on the CQD surface to form a recognition unit, which showed high sensitivity and selectivity toward Cu^{2+} over other metal ions.[114] Gedda *et al.* reported the use of prawn shell biomass for the synthesis of CQDs, which were further used as selective sensors for Cu^{2+} ions with an LOD value of 5 nM. The high selectivity of CQDs towards Cu^{2+} compared to other metal ions was due to the high affinity of Cu^{2+} ions towards the amine groups present on the surface of CQDs.[115]

Mercury ion detection

Mercury ions are one of the major contaminants due to their high toxic nature, and are responsible for various human disorders including mitosis impairment, DNA damage, kidney toxicity and sometimes permanent damage to endocrine and nervous systems.[116] Even after the removal of the pollutant source, the Hg^{2+} ions tend to remain in the system for a larger time and lead to poisoning.[117] The maximum allowable level of Hg^{2+} in drinking water is 10 nM. It is thus essential to develop sensitive and selective sensors. Which can detect mercury ions at a very low concentration. Several CQDs synthesized using green carbon sources have been reported for Hg^{2+} ion detection and their addition to CQDs resulted in their fluorescence quenching. Wenbo Lu *et al.* reported the synthesis of CQDs using pomelo peel and utilized them as sensors for Hg^{2+} ions in water samples. The electron transfer process among CQDs and metal ions was proposed as a probable fluorescence quenching mechanism, which was further proven by eliminating Hg^{2+} from the CQD surface *via* a chelator.[40] Qin, *et al.*, reported the synthesis of CQDs of 1–4 nm size using flour as the carbon precursor having a QY of 5.4%. The prepared CQDs were used as fluorescent sensing probes for the detection of Hg^{2+} ions with an LOD value of 0.5 nM in the linear range of 0.0005–0.01 M. The high selectivity and sensitivity of these CQDs towards Hg^{2+} ions attributed to strong affinity between Hg^{2+} ions and carboxylic groups on the CQD surface. It was found that the PL intensity of these CQDs is pH sensitive and increases with the increase in pH values. In an acidic medium, the CQDs showed low quenching efficiency due to the breaking of CQD–Hg^{2+} complexes *via* protonation of the surface-binding carboxyl groups. However, deprotonation occurs at high pH and carboxylate groups present on CQDs strengthen the interaction between CQDs and Hg^{2+} ions.[118] Gu, *et al.* reported the synthesis of fluorescent N-CQDs using lotus root as the carbon source having a nitrogen content of 5.23%. These N-doped CQDs have a diameter of 9.41 nm and used as a sensor for the detection of Hg^{2+} ions and cell imaging. The N-CQDs efficiently detect Hg^{2+} ions in a linear range from 0.1 to 60.0 μM with an LOD value of 18.7 nM.[32] The graphical representation of CQD synthesises and their characterisation using lotus root is shown in Fig. 12.

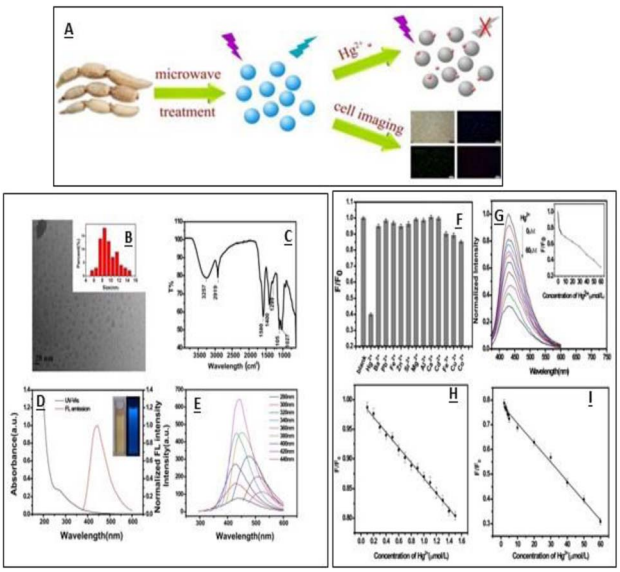

Fig. 12 (A) Synthesis of CQDs. (B) TEM spectra of the synthesised CQDs. (C) FTIR spectra of CQDs. (D) UV-vis and fluorescence emission spectra of CQDS. (E) Emission spectra of CQDs at different excitation wavelengths. (F) Fluorescence response of CQDs towards different metal ions. (G) Fluorescence spectra of CQDs at different Hg^{2+} concentrations (H). (I) Relationship between the F/F_0 and Hg^{2+} concentrations. Reproduced from ref. 32 with permission from Elsevier, copyright 2023.

Yadian *et al.*, reported a green method for the synthesis of water-soluble N-CQDs using ethane diamine as the nitrogen source and barley as the carbon source with a QY of 14.4%. These blue fluorescent N-CQDs showed selective detection of Hg^{2+} ions in the range of 10–160 μM with an LOD value of 0.48 μM. The quenching of fluorescence is attributed to the interaction between Hg^{2+} and carboxylic group present on the N-CQD surface.[119] Li *et al.* used Hongcaitai as the carbon source for the synthesis of CQDs using hydrothermal treatment. These CQDs showed the selective detection of ClO^- and Hg^{2+} ions.[120] Hasan and co-worker reported the synthesis of CQDs using *Tamarindus indica* leaves having a QY of 46.6%. These CQDs were used as selective nano-probes for the turn-off sensing of Hg^{2+} with an LOD value of 6 nM in the dynamic range of 0–0.1 μM.[121]

Lead ion detection

Lead is considered as a hazardous metal causing many disorders in the human body and posing a threat to the environment. It occurs mainly in three oxidation states, *i.e.*, Pb(0), Pb(II) and Pb(IV). The main source of lead ions in drinking water is the use of service pipes containing lead and other relevant accessories, which corrode in the presence of acidic water. The lead uptake

Fig. 13 Synthesis of CQDs using lemon peels *via* a hydrothermal treatment.[125]

Table 1 Metal ion sensing by CQDs

Entry no.	Carbon source	Synthesis method	Average size (nm) and color	Quantum yield (%)	Metal ion	Linear range	LOD values	References
1	Lotus root	Microwave	9.41 Blue	19.0	Hg^{2+}	0.1–60 μM	18.7 nM	32
2	Broccoli	Hydrothermal	2–6 Blue	NA	Ag^{+}	0–600 μM	0.5 μM	39
3	Pomelo peel	Hydrothermal	2–4 Blue	6.9	Hg^{2+}	NA	0.23 nM	40
4	Finger millet ragi	Pyrolysis	3–8 Blue	NA	Cu^{2+}	0–100 μM	10 nM	48
5	Lantana camara berries	Hydrothermal	5 ± 3 Blue	33.1	Pb^{2+}	0–200 μM	9.64 nM	50
6	Peach gum polysaccharides	Hydrothermal carbonization	2–5 Blue	28.46	Au^{3+}	0–50 μM	0.64 μM	67
7	Sago waste	Thermal pyrolysis	6–17 Blue	NA	Pb^{2+} Cu^{2+}	NA	7.49 μM 7.78 μM	69
9	D-Glucose	Simple heating method	>20 Green	NA	Pb^{2+}	0.010–0.030 μM	0.014 μM	70
10	Grilled turbot fish	Microwave heating	3–5 Blue	1.67	Fe^{3+}	20–110 μM	3.96 μM	71
11	Coriander leaves	Hydrothermal	2.38 Blue	6.48	Fe^{3+}	0–60 μM	0.4 μM	73
12	Bamboo leaves	Hydrothermal	3.6 Blue	7.1	Cu^{2+}	0–66 μM	0.115 μM	74
13	Sweet potato	Hydrothermal	3.39 Blue	8.64	Fe^{3+}	1–100 μM	0.32 μM	84
14	Table sugar	Microwave	3.5 Blue	2.5	Pb^{2+}	NA	67 μM	88
15	Jackfruit seeds	Microwave	3–7 Blue	17.91	Au^{3+}	0–100 μM	239 nM	89
16	Waste tea	Hydrothermal	10 Blue	7.1	Fe^{3+}	53.5–267.5 μM	0.15 μM	95
17	Pineapple peel	Hydrothermal	2–3 Blue	42.0	Hg^{2+}	0.1–100 μM	4.5 nM	96
18	Chocolate	Hydrothermal	6.41 Blue	NA	Pb^{2+}	0.033–1.67 μM	12.7 nM	97
19	Coconut water	Microwave-assisted hydrothermal method	1–6 Blue and green	2.8	Cu^{2+}	10–50 μM	0.280 μM	98
20	Pipe tobacco	Hydrothermal	5 Blue	3.2	Cu^{2+}	0–40 mM	0.01 μM	99
21	*Mexican mint*	Microwave-assisted reflux method	2.43 ± 0.02 Blue	17	Fe^{3+}	0–15 μM	0.53 μM	103
22	*Prunus cerasifera*	Hydrothermal	3–5 Blue	NA	Fe^{3+}	0–0.5 mM	NA	104
23	Vitamin B1	Hydrothermal	3.2 Blue	4.4	Fe^{3+}	0.1–1.00 mM	177 nM	105
24	*Blueberry*	Liquid N_2 treatment and centrifuge processes	NA	NA	Fe^{3+}	12.5–100 μM	9.97 μM	106
25	*Watermelon juice*	Hydrothermal carbonization	3–7 Blue	10.6	Fe^{3+}	0–300 μM	0.16 μM	107
26	*Rose-heart radish*	Hydrothermal treatment	1.2–6 Blue	13.6	Fe^{3+}	0.02–40 μM	0.13 μM	108
27	Mangosteen pulp	Hydrothermal	5 Blue	2.8	Fe^{3+}	0–0.18 mM	52 nM	109
28	*Boswellia ovalifoliolata* bark	Hydrothermal-carbonization	4.16 ± 0.22 Green	10.2	Fe^{3+}	0–500 μM	0.41 μM	110
29	Banana juice	Hydrothermal	1.27 Blue	32	Cu^{2+}	1–800 μg mL^{-1}	0.3 μg mL^{-1}	112
30	Prawn shell	Hydrothermal	4 Blue	9	Cu^{2+}	0.1–5 μM	5 nM	115
31	Flour	Microwave	1–4 Blue	0.5	Hg^{2+}	0.0005–0.01 μM	0.5 nM	118

Table 1 (*Contd.*)

Entry no.	Carbon source	Synthesis method	Average size (nm) and color	Quantum yield (%)	Metal ion	Linear range	LOD values	References
32	Highland barley	Hydrothermal	5.8 Blue	14.4	Hg^{2+}	10–160 μM	0.48 nM	119
33	Hongcaitai	Hydrothermal	1.6–2.3 Blue	12.1	Hg^{2+}	0.2–15 μM	60 nM	120
34	*Tamarindusindica* leaves	Hydrothermal	3.4 ± 0.5 Blue	46.6	Hg^{2+}	0–0.1 μM	6 nM	121
35	Potato-dextrose agar	Microwave	4.3 Blue	9.0	Pb^{2+}	0–20 μM	0.11 nM	122
36	Ocimum sanctum leaves	Hydrothermal	3.0 Green	9.3	Pb^{2+}	10–1000 μM	0.59 nM	123
37	Bamboo leaves	Solvothermal	3–7 Red	4.7	Pb^{2+} Hg^{2+}	0.6–800 nM 1–1000 nM	0.14 nM 0.22 nM	124
38	Lemon peel waste	Hydrothermal	1–3 Blue	14	Cr^{4+}	2.5–50 μM	73×10^{-3} μM	125
39	Quince fruit	Microwave	4.85 ± 0.07 Blue	8.55	As^{3+}	0.5–10 μM	0.01 μM	126
40	Edible prickly pear cactus	Hydrothermal	5.6 Blue	12.7	As^{3+}	$2–12 \times 10^{-3}$ μM	2.3×10^{-3} μM	127
41	*Nerium Oleander* L. Petals	Hydrothermal	1–9	3.5	Co^{2+}	6.45×10^{-3} μM	0–40 μM	128
42	Kelp	Microwave	3.7 Blue	23.5	Co^{2+}	1–200 μmol L^{-1}	0.39 μmol L^{-1}	129
43	*Pyrus pyrifolia* fruit	Hydrothermal	2.0 ± 1.0 Blue	10.80	Al^{3+}	0.005–50 μM	0.0025 μM	130
44	Honey	Solvothermal	2 Blue	19.8	Fe^{3+}	5.0×10^{-9} to 1×10^{-4} mol L^{-1}	1.7×10^{-9} mol L^{-1}	131
45	Pseudostem of banana	Hydrothermal	2.5 Blue	48	Fe^{3+}	0–100 μM	6.4×10^{-3} μM	132
46	Sugarcane molasses	Hydrothermal	1.9 Blue	5.8	Fe^{3+}	0–20 μM	1.46 μM	133
47	Onion waste	Autoclave	15 Blue	28	Fe^{3+}	0–20 μM	0.31 μM	134
48	Coffee beans	Hydrothermal	4.6 Blue	9.8	Fe^{3+}	0–0.10 mM	15.4–16.3 nM	135
49	Tomato	Chemical oxidation	5.0–10.0 Blue, green and yellow	12.70	Fe^{3+}	0.1–2.0 μM	0.016 μM	136
50	Soybeans	Ultrasonic	2.4 Blue	16.7	Fe^{3+}	0–30 μM	2.9 μM	137
51	*Magnifera indica* leaves	Pyrolysis	2–10 Blue	18.2	Fe^{3+}	NA	3.12 μM	138
52	Ripe banana peels	Hydrothermal	6.9 Blue	27	Fe^{3+}	121×10^{-6} μM	$10–200 \times 10^{-6}$ μM	139
53	Dried rose petals	Hydrothermal	6–9 Green	28	Cr^{4+}	$10–200 \times 10^{-6}$ μM	81×10^{-6} μM	139
54	Curaua fibers	Hydrothermal	2.4 Blue	NA	Fe^{3+}	0.77 μM	0–30 μM	140
55	Lycii fructus	Hydrothermal	2–5 Blue	17.2	Fe^{3+}	0–30 μM	21×10^{-3} μM	141
56	Dwarf banana peel	Hydrothermal	4 Blue	23.0	Fe^{3+}	5–25 μM	0.66 μM	142
57	*Bombyx mori* silk	Hydrothermal	5.6 Blue	61.1	Fe^{3+}	0.5–4 μM	0.38 μM	143
58	Syringa oblata lindl	Hydrothermal	1.0–5.0 Blue	12.4	Fe^{3+}	0.5–80 μM	0.11 μM	144
59	Rice residue	Hydrothermal	2.70 Blue	23.48	Fe^{3+}	3.3–32.2 μM	0.7462 μM	145
60	Lemon juice	Hydrothermal	20 Blue	38	Fe^{3+}	1–90 μM	2.5 μM	146

Table 1 (*Contd.*)

Entry no.	Carbon source	Synthesis method	Average size (nm) and color	Quantum yield (%)	Metal ion	Linear range	LOD values	References
61	Kiwi fruit peels	Hydrothermal	5.6 Blue	14	Fe^{3+}	5–25 μM	0.95 and 0.85 μM	147
62	Betel leaves	Hydrothermal	4 Blue	4.21	Fe^{3+}	0.3–3.3 μM	0.135 μM	148
63	*Prunus avium* fruit	Hydrothermal	7 Blue	13	Fe^{3+}	0–100 μM	0.96 μM	149
64	*Magnolia liliiflora* flower	Hydrothermal	4 ± 1 Blue	11	Fe^{3+}	0–25 μM	1.2 μM	150
65	Coconut water	Stirrer-assisted route	5 Blue	14.34	Fe^{3+}	0–700 μM	0.30 μM	151
66	Pinewood	Hydrothermal	3.56 Blue	4.69	Fe^{3+}	0–2000 mmol L^{-1}	355.4 nmol L^{-1}	152
67	Lychee waste	Solvothermal	3.13 Blue	23.5	Fe^{3+}	0–22 μM	23.6 nM	153
68	Betel leaf	Hydrothermal	3.7 Blue	4.21	Fe^{3+}	0.3–3.3 μM	0.135 μM	154
69	Papaya powder	Hydrothermal	3.4–10.8	18.98	Fe^{3+}	1–10 μmol L^{-1}	0.48 μmol L^{-1}, 0.29 μmol L^{-1}	155
	W-CQDs		Blue	18.39		1–8 μmol L^{-1}		
	E-CQDs							
70	Brewer's spent grain	Microwave synthesis	5.3 ± 2.4 Blue	14	Fe^{3+}	NA	0.05 μM	156
71	Poa pratensis	Hydrothermal	9 Blue	7	Fe^{3+}, Mn^{2+}	5.0–25 μM	1.4–1.2 μM	75
72	Cranberry beans	Hydrothermal	1.23–6.63 Blue	10.85	Fe^{3+}	30–600 μM	9.55 μM	157
73	*Catharanthus roseus*	Hydrothermal carbonization	5 Blue	28.2	Fe^{3+}	0–6 μM	0.3 μM L^{-1}	158
74	Cat feed stock	Hydrothermal carbonization	NA	NA	Fe^{3+}	12.5–100 μM	32 μM	159
75	Mango-peel	Pyrolyzation with oxygenolysis	2–6 Blue	8.5 ± 0.2	Fe^{3+}	4–16 μM	1.2 μM	160
76	Fuel waste	Oxidative acid treatment	5	3	Fe^{3+}	NA	0.65 μM	161
77	Waste kitchen chimney oil	Ultrasonication	1–4 Blue	7.5	Fe^{3+}	0.001–600 μM	0.00018 μM	162
78	Black tea	Hydrothermal	4.6 Blue	NA	Fe^{3+}	0.25–60 μM	0.25 μM	163
79	Goose feather	Microwave-hydrothermal treatment	21.5 Blue	17.1	Fe^{3+}	1–14 μM	0.196 μM	164
80	*Fusobacterium nucleatum*	Hydrothermal carbonization	4.06 Blue	9.99	Fe^{3+}	20–180 mM	0.82 μM	165
81	Corn bract leaves	Solvothermal	2.6 Blue	6.90	Hg^{2+}	0–40 μM	9 nM	166
82	*Prosopis juliflora* leaves	Carbonization	5.8 Blue	5.0	Hg^{2+}	5–500 ng mL^{-1}	1.26 ng mL^{-1}	167
83	Strawberry juice	Hydrothermal	5.2 Blue	6.3	Hg^{2+}	0.001–50 μM	3 nM	168
84	China grass carp scales	Microwave supported hydrothermal	2.6 ± 0.8 Blue	19.9	Hg^{2+}	0.014–30 μmol L^{-1}	0.014 μmol L^{-1}	169
85	Honey	Hydrothermal	2–4	NA	Hg^{2+}	0–10 × 10^{-3} μM	1.02 nM	170
86	Jinhua bergamot	Hydrothermal	10 Blue	50.7	Hg^{2+}	0.01–100 μM	5.5 nM	171
87	Coconut milk	Thermal pyrolysis	20–50 Blue	NA	Hg^{2+}	30.5 × 10^{-3} μM	16.5 nM	172
88	Cucumber juice	Hydrothermal	2.8–4.0 Blue	3.5	Hg^{2+}	1–70 μM	180 nM	173

Table 1 (*Contd.*)

Entry no.	Carbon source	Synthesis method	Average size (nm) and color	Quantum yield (%)	Metal ion	Linear range	LOD values	References
89	Muskmelon	Acid oxidation	2–5 Blue 3.5–6 Green 4.5–7 Yellow	26.9	Hg^{2+}	1.0–25 μM	330 nM	174
90	*Dunaliella Salina*	Hydrothermal	4.7 Blue	8	Hg^{2+}	0.03–0.20 μM	18 nM	175
91	Chinese yam	Hydrothermal	2.7 ± 1.4 Blue	9.3	Hg^{2+}	10–30 × 10^{-3} μM	1.26 nM	176
92	Lemon juice	Hydrothermal	Blue	2.4	Hg^{2+}	0–1.82 × 10^{3} μM	36 × 10^{3} nM	177
93	Corn flour	Hydrothermal	3.5 Blue	7.7	Cu^{2+}	NA	0.001 μM	178
94	Human urine	Thermal treatment	10–30 Blue	5.3	Cu^{2+} Hg^{2+}	NA	3.4 μM 2.7 μM	179
95	Peanut shells	Pyrolysis	1.8–4.2 Blue	10.58	Cu^{2+}	0–5 μM	4.8 μM	180
96	Lemon juice	Thermal coupling	3.5 Blue	7.7	Cu^{2+}	0–15 μM	0.047 μM	181
97	Kelp	Hydrothermal	4.5 Blue to deep-green	12.3	Cu^{2+}	1–12.5 μM	7 × 10^{-3} μM	182
98	Grass	Hydrothermal	3–5 Blue	4.2	Cu^{2+}	0–50 μM	1 × 10^{-3} μM	183
99	Pu-erh tea	Brewing method	NA Blue	NA	Cu^{2+}	0–22 μM	51 × 10^{-3} μM	184
100	*Petroleum coke*	Ultrasonic-assisted chemical oxidation	2.0–4.5 NA	9.8	Cu^{2+}	0.25–10 μM	0.0295 μM	185
101	Celery stalk	Hydrothermal	3.7 ± 1.1 Blue	NA	Cu^{2+}	0–100 μM	0.132 μM	186
102	Pear juice	Hydrothermal	10 Blue	NA	Cu^{2+}	0.1 mg L^{-1} to 50.0 mg L^{-1}	0.1 mg L^{-1}	187
103	Pineapple juice	Hydrothermal	NA Blue	10.06	Cr^{4+}	0–18 μM	0.052 μM	188
104	Papaya waste (*Carica papaya*)	Pyrolysis	7 Blue	23.7	Cr^{3+} Cr^{4+}	0.028–2.86 μM	2 × 10^{-3} μM	189
105	Tulsi leaves	Hydrothermal	5 Blue	3.06	Cr^{4+}	1.6–50 μM	0.015 μM	190
106	Kelp	Hydrothermal	2–4 Blue	20.5	Cr^{4+}	0.01–50 μM	0.52 μM	191
107	Denatured milk	Hydrothermal	2 Blue	NA	Cr^{3+}	NA	14 μM	192
108	Black particulates of petrol soot	Oxidation	1.5 green	NA	Cr^{4+}	0–20 × 10^{3} μM	0.51 μM	193
109	Groundnut	Hydrothermal	2.5	17.6	Cr^{3+}	2–8 μM	1.9 μM	194
110	Edible seeds	Pyrolysis route	5–10	41.8	Cr^{3+}	1–14 μM	1.3 μM	195
111	Biomass	Hydrothermal	∼2.4 Blue	22.6	Pb^{2+}	1.3–106.7 μM	NA	196
112	Ginkgo biloba leaves	Hydrothermal	4.18 ± 1.14 Blue	16.1	Pb^{2+}	0.1–20.0 × 10^{-3} μM	0.055 nM	197
113	Black tea	Hydrothermal	1.0–3.0 nm	NA	Pb^{2+}	NA	13.3 nmol L^{-1}	198
114	Pomegranate juice	Hydrothermal	2–5 Blue	NA	Ag^{+}	8.3 × 10^{-4} μM	38 × 10^{-3} μM	199
115	Neem leaves	Pyrolysis and hydrothermal	5–6 Green and blue	54	Ag^{+}	NA	0.2–0.6 × 10^{3} μM	200
116	Gum tragacanth	Hydrothermal	1–1.5 Blue and green	66.74	Au^{3+}	0–100 μM	2.69 μM	201

Table 1 (*Contd.*)

Entry no.	Carbon source	Synthesis method	Average size (nm) and color	Quantum yield (%)	Metal ion	Linear range	LOD values	References
117	*Syzygium cumini*	Hydrothermal	2.1 ± 0.7	6.1	Mn^{2+}	0.0075–0.1 mM	2.1 μM	202
118	Durian shell waste	Hydrothermal carbonisation	10 Blue	28.7	Mn^{7+}	0–100 μM	46.8 nM	203
119	*Osmanthus fragrans*	Hydrothermal	NA Blue	21.9	Al^{3+}	0.1–100 μM	26 nM	204
120	Potato starch	Acid-assisted ultrasonic route	3–5 Green	10.0	Zn^{2+}	0–20 μM	1 nM	205
121	Linter extract	Hydrothermal	1.15 ± 0.30	6.21	Zn^{2+}	NA	6.4 μM	206
122	Whey (major dairy waste)	Pyrolysis	4 Blue	∼11.4	Se^{4+}	10–50 μg L^{-1}	8.48 × 10^5 M^{-1}	207
123	Lemon juice	Hydrothermal	4–5 Green	21.0	V^{5+}	0–8 ppm	3.2 ppm	208
124	Roasted chickpeas	Microwave	4.5–10.3 Blue	1.8	Fe^{3+}	11.25–37.50 μM	2.74–8.22 μM	209
125	Gelatin	Hydrothermal	0.5–5 Blue	22.7	Fe^{3+}	0–50 μM	0.2 μM	210
126	Rice husks	Hydrothermal	1.5–3	NA	Cd^{2+}	NA	NA	211
127	Cabbage	Hydrothermal	2–4 Blue	NA	Fe^{3+} Hg^{2+} Pb^{2+}	NA	NA	212
128	Eggshell membrane	Hydrothermal	8 Blue	9.6	Hg^{2+}	10–100 μM	2.6 μM	213
129	Oyster mushroom (pleurotus species)	Hydrothermal carbonization	8 Blue and green	NA	Pb^{2+}	10–200 μM	58.63 μM and 177.69 μM	214
130	Seville orange	Hydrothermal	4.8 Blue	13.3	Fe^{3+}	0.033–0.133 mM	0.53 μM	215
131	Shrimp shells	Calcination	3–5 NA	20	Cr^{6+}	0–70 mM	0.1 μM	216
132	Luffa sponge based activated carbon fibre	Chemical oxidation	6.8 Green	2.1	Cr^{6+}	NA	NA	217
133	*Murrayakoenigii* leaves	Hydrothermal	2–8 Blue	5.4	Cd^{2+}	0.01–8 μM	0.29 nM	218
134	Coconut sap	Hydrothermal	1–7	NA	Ag^{+}	1–70 μM	0.26 μM	219
135	White wasted foam	Hydrothermal	6–8 Multi-color	NA	Cr^{3+}	NA	6 μM	220
136	Crown daisy leaves	Hydrothermal	5.0–10.0 Blue	NA	Cu^{2+}	10.0–120.0 nM	1.0 nM	221
137	Red beetroot	Hydrothermal	5–7 Green	27.6	Pd^{2+}	3–43 μM	33 nM	222
138	Rice starch	Hydrothermal	11	3.2	Hg^{2+}	3.3 × 10^{-7} to 50.0 × 10^{-6} mol L^{-1}	1.8 × 10^{-7} mol L^{-1}	223
139	Kumquat	Hydrothermal	1.5–4 Blue	0.08	Fe^{3+}	0–40 μM	0.70 μM	224
140	Rambutan and Pandan leaves	Hydrothermal and microwave treatment	NA	2.46 and 2.70	Cu^{2+}	NA	123 μM	225
141	Flax straw	Hydrothermal	2.2 Blue–green	20.7	Co^{2+} and Cr^{6+}	0–500, 0.5–80 μM	0.38, 0.19 μM	226
142	*Tagetes erecta*	Hydrothermal	4–6 Blue	NA	Fe^{3+}	0–90 μM	0.36 μM	227
143	*Volvariella volvacea* mushroom	Hydrothermal	5.8 Blue	11.5	Fe^{3+} and Pb^{2+}	1–100 μM	12 and 16 nM	228
144	Quinoa saponin	Hydrothermal	2.25 Blue	22.2	Co^{2+}	20–150 μM	0.49 μM	229
145	Betel leafs (*Piper betle*)	Hydrothermal	3–7 Blue	NA	Fe^{3+}	0–150 nM	50 nM	230
146	Grape seeds	Hydrothermal	8.9	27.5	Cu^{2+}	150–500 μg mL^{-1}	0.048 mg L^{-1}	231

Table 1 (*Contd.*)

Entry no.	Carbon source	Synthesis method	Average size (nm) and color	Quantum yield (%)	Metal ion	Linear range	LOD values	References
147	Maple tree leaves	Hydrothermal	2–10 Blue	NA	Cs^{+}	100–100 nM	160 nM	232
148	*Sugarcane waste*	Hydrothermal	2–6 Blue	3.34	Hg^{2+}	0–300 μM	0.1 μM	233
149	*Borassus flabellifer*	Hydrothermal	2–7 Blue	19.4	Fe^{3+}	10–100 μM	2.01 μM	234
150	*Wolfberry*	Hydrothermal	1.55 ± 1 Blue	22	Fe^{3+}	3 and 100 μmol L^{-1}	3 μmoL L^{-1}	235
151	Wool keratin	Hydrothermal	2–6 Blue	NA	Cr^{6+} and Fe^{3+}	2.5–50 μM 0.25–125 μM	14.16 nM 113 nM	236
152	Water hyacinth	Hydrothermal	1.2–4.2 Blue	3.3	Fe^{3+}	0–330 μM	0.084 μM	237
153	Manihot esculenta	Hydrothermal	3–5 Blue	NA	Fe^{3+}	10–100 μM	13.65 μM	238
154	Crab-shell	Hydrothermal	10 Green	NA	Cd^{2+}	50–250 μM	—	239
155	Lignocellulosic agro-forest biomass	Hydrothermal	2–6 Blue	1.66	Fe^{3+}	15.6–62.5 μM	0.91 μM	240
156	*Poria cocos*	Hydrothermal	4.61 Blue	4.82	Cr^{6+}	1–100 μM	0.25 μM	241
157	Pig bones	Hydrothermal	1–4 Blue	26.4	Co^{2+}	0–15 μg mL^{-1} and 30–80 μg mL^{-1}	20 μg L^{-1}	242
158	Corn straw	Hydrothermal	5 nm	4.64	Cu^{2+}	1–20 mg L^{-1} and 20–500 mg L^{-1}	4.26 mg L^{-1}	243
159	Canon ball fruit	Hydrothermal	11.2 Blue	7.01	Fe^{3+}	0.6–3.3 μM	0.071 μM	244
160	Magnolia grandiflora	Hydrothermal	12 Blue	NA	Ni^{2+}	1–10 μM	0.9 μM	245
161	Avocado seeds	Carbonisation	4.6–3.2 Blue	9.2	Cu^{2+}/Cr^{6+}	1.5–4 μM 30–200 μM	0.09 nM 0.04 nM	246
162	Tea leaves	Hydrothermal	2.0–2.5 Blue	NA	Fe^{3+}	0.1–400 μM	0.079 μM	247
163	*Morus nigra* fruit	Hydrothermal	3–6 Blue	24	Fe^{3+}	5–30 μm	0.47 μM	248
164	Grapefruit juice	Hydrothermal	3.8 Blue	84.93	Cr^{4+}	0–400 μM	0.155 μM	249
165	*Lycium ruthenicum*	Hydrothermal	3.0–6.5	21.8	Ag^{+}	0.7–36 μM	59 nM	250
166	Grass	Reflux method	20 NA	NA	Cu^{2+}	1–20 μM	0.89 μM	251
167	*Myrica rubra*	Hydrothermal	1.72–4.58 nm Blue	54	Fe^{3+}	1–1000 mM	0.3 μM	252
168	*Pseudomonas aeruginosa*	Hydrothermal carbonization	2–6 Blue	10.2	Cr^{6+}	0–9 μM	0.23 nmol L^{-1} (nM)	253
169	*Curcuma amada*	Hydrothermal	7 Blue	NA	Hg^{2+}	1–10 nM	0.2 nM	254
170	*Gum ghatti*	Microwave pyrolysis	1–7 Blue	23	Hg^{2+}	0–30 μM	4.6 nM	255
171	Neem seed	Microwave heating	∼2 nm Blue	∼12.5	Au^{3+}	NA	∼16 nM	256
172	Maize starch	Solvothermal	NA Blue	6.2	Cr^{4+}	0–25 μmoL L^{-1}	0.34 μmoL L^{-1}	257
173	*Tinospora cordifolia* leaves	Hydrothermal carbonization	5.47 Blue	3.7	Fe^{3+}	0.237–0.67 mg mL^{-1}	0.414 μM	258
174	Canistel (*Pouteria campechiana*)	Hydrothermal	∼8.1 Blue	1.24	Fe^{3+}	27–2700 μM	19.0 μM	259
175	Wheat straw	Carbonization	1.73 Blue	NA	Cu^{2+}	0–200 μM	3.23 μM	260

Table 1 (*Contd.*)

Entry no.	Carbon source	Synthesis method	Average size (nm) and color	Quantum yield (%)	Metal ion	Linear range	LOD values	References
176	Natural rubber	Pyrolysis and hydrothermal method	2.4 Blue	0.6	Mg^{2+}	0–250 μM	4.3 μM	261
177	Elm seeds	Hydrothermal	3.83 Blue	6.15	Fe^{3+}	0–500 μM	3.18 μM	262
178	*Crescentia cujete* fruit waste	Hydrothermal	4.36 Blue	1.57	Fe^{3+}	0–25 μM	0.257 μM	263
179	*Polyalthia longifolia*	Hydrothermal	3.33 Red	22	Cd^{2+}	2.4 nM	7.3 nM to 12 μM	264
180	*Vitex negundo* leaves	Hydrothermal	6.5 Blue	12.2	Mn^{2+}	1.25 nM	10.0–50.0 nM	265
181	Spent coffee grounds	Ball milling	1.64 ± 0.04 Blue	3.95	Fe^{3+}	2.25 μM	(0–2 mM)	266
182	Chebulic myrobalan	Hydrothermal carbonization	2.5 ± 0.5 Blue	15	Fe^{3+}	0.86 μM	5–25 μM	267
183	*Annona reticulata* leaves	Hydrothermal	6 Green	12	Cr^{3+}	2 μM	0 to 40 μM	268
184	Pine needles	Hydrothermal	3.56 ± 0.85 Blue	7.65	Fe^{3+}	0.02 μM	0.1–540 μM	269
185	Cow milk	Hydrothermal	1–2 Blue	59.47	Fe^{3+}	0.1–20 μmol L^{-1}	0.6 μmol L^{-1}	270
186	Prickly pear	Microwave-assisted	2.0 ± 0.5 Blue	14.8	Cr^{4+}	0–150 μM	0.04 μM	271
187	*Delonix regia* leaves	Hydrothermal	6.75 ± 2.5 Red	7	Pb^{2+}	10–180 μM	3.3 nM	272

limit in drinking water has been reported to be ~15.0 ppb.[122] Several inorganic nanomaterials such as ZnS, gold, CdS, polymer dots, and enzyme-based sensors have been utilized as fluorescent probes for the detection of Pb^{2+} ions. However, such methods have drawbacks of high cost. Thus, the development of low-cost and eco-friendly materials for the sensing of Pb^{2+} continues to be an active area of research. CQD-based sensors have attracted considerable attention due to their eco-friendly synthetic approaches. Kumar *et al.* reported the CQDs synthesized using *Ocimum sanctum* and used them for the detection of Pb^{2+} in real water samples. The quenching of fluorescence emission intensity was observed in the presence of Pb^{2+} ions with an LOD value of 0.59 nM and a QY of 9.3%. The decrease in the fluorescence intensity of CQDs attributed to the electron–hole recombination, which occurs due to the high binding affinity between the empty d-orbital of Pb^{2+} ions and the amine group present on the CQD surface.[123] N-CQDs have been prepared using *Lantana camara* berries thoroughly studied for FL quenching mechanism for both dynamic and static processes. The results of Stern–Volmer plots obtained at three different temperatures confirm the direct relation between the quenching constant and temperature. These N-CQDs efficiently sense Pb^{2+} ions in human urine and serum as well as in water samples. With the increase in Pb^{2+} concentration, a decrease in the fluorescence intensity at 450 nm was observed, confirming the selectivity of CQDs towards Pb^{2+}.[50] CQDs having an average size of 3.5 nM have been synthesized using sugar for the sensing of Pb^{2+} ions. Carboxylate group-induced aggregation process has been responsible for fluorescence quenching, which was confirmed by FTIR and XRD data. These CQDs have also been used for the detection of Pb^{2+} ions in real water samples.[88] Furthermore, fluorescent CQDs synthesized with bamboo leaves have been used for the selective detection of Pb^{2+} ions in river water and further employed for environmental monitoring for water safety and waste management.[124]

Other cation detection

CQD-based fluorescent sensors have been reported for other heavy metal ions besides those discussed above. Several mechanisms have been reported for the detection of different metal ions using CQD-based sensors, which might be due to the presence of different functional groups on CQDs since they have been synthesized using different carbon precursors. Tyagi *et al.* reported the synthesis of spherical shaped water-soluble CQDs of 1–3 nm size using lemon peel waste as the carbon source with a QY of 14%. These CQDs showed good water solubility due to the presence of oxygen-containing groups on their surface. Further, these CQDs were used as "turn off" fluorescent probes for the detection of Cr^{6+} ions in aqueous solutions with an LOD value of ~73 nM. The higher selectivity of CQDs towards Cr^{6+} ions is due to a higher thermodynamic affinity in the concentration range of 2.5–50 μM with a linear response.[125] The schematic representation of CQDs synthesis using lemon peel waste is shown in Fig. 13.

Arumugam *et al.* reported the selective detection of Ag^{+} ions using water-soluble fluorescent CQDs synthesised from broccoli. These CQDs exhibit bright blue luminescence with an LOD value of 0.5 μM for Ag^{+} ions.[39] Yu *et al.* reported the synthesis of N-CQD from *Osmanthus fragrans* with a QY of 21.9%. Further, these N-CQDs were used as fluorescent nano sensors for Al^{3+} ions. The sensing ability was found to be in the range of 0.1–100 μmoL L^{-1} towards Al^{3+} ions with an LOD value of 26 nmoL L^{-1}.[42] Quince fruit has been utilized for the synthesis of CQDs, and the influence of various anions and cations on the PL quenching of prepared CQDs was investigated. It was found that MnO_4^{-} and Fe^{3+} exhibit intense effects on the PL properties. Oxidising agents such as $KMnO_4$ are capable of introducing holes into CQDs, which further leads to an increased population of holes in CQDs and speeds up electron–hole annihilation, resulting in energy release in the form of chemiluminescence emission while simultaneously decreasing the fluorescence intensity of CQDs at the maximum emission wavelength. Additionally, it has been found that at varying pH levels, permanganate can also oxidise As^{3+}. Considering these phenomena, the potential application of synthesised CQDs for As^{3+} ions was evaluated.[126] Radhakrishnan *et al.* reported the sensing of As^{3+} ions by CQDs synthesized using prickly pear cactus fruit passivated with glutathione. The quenching mechanism was investigated to be static in nature.[127] Dutta *et al.* synthesised N-CQDs using ethylene diamine (as nitrogen source) and *Nerium Oleander* L. Petals (as carbon source). The emission intensity of Rhodamine 6G and N-CQD systems gets quenched after the addition of Co^{2+} ions, most probably due to the hindrance of the FRET mechanism.[128] Further, Zhao *et al.* reported N-CQDs synthesized using kelp and ethylenediamine for the detection of Co^{2+} ions in real water samples. IFE was reported as a plausible fluorescence quenching mechanism, which was confirmed through the overlapping of absorption and emission signals and lifetime measurements.[129] Hydrothermally synthesised CQDs using pear fruit were utilised as ''turn-on'' sensors for the detection of Al^{3+} ions in real water samples and found to follow chelation-enhanced fluorescence emission mechanism (CHEF). The interactions of carboxylic and amine groups on CQDs with Al^{3+} ions have been used to explain the CHEF process. Au^{3+} ion sensing in real river water has been reported using N-CQDs synthesized from natural peach gum polysaccharide and ethylenediamine.[130] Several different metal ions detected using green CQD-based sensors are summarised in Table 1.

Conclusions and future perspective

The studies reported in the literature revealed that the CQDs are one of the fascinating materials of the 20th century due to their inherent physical and chemical properties. Their easy synthetic procedure and low cost of synthesis are the additional advantages. This review presented the recent progress in green synthesis of CQDs and their applications for heavy metal ion sensing. The functional groups present on the surface of CQDs have been found to be dependent on the green precursor used for their synthesis. The major factors influencing the synthesis of CDs include molecular state, surface state, as well as the quantum confinement effects, and these factors can be easily controlled by altering the strategies for CD synthesis. During the synthesis of CDs, several functional groups such as amine, epoxy, ether, carbonyl, carboxyl, and hydroxyl can be incorporated. Besides, the surface of CDs can be easily functionalized by doping them with heteroatoms such as N, P, S, and B using various biological, polymeric, and organic materials. Henceforth, the properties of CDs can be regulated by varying the size and extent of the surface functional groups by either adapting different synthesis techniques or using other precursors. The modification of CDs is crucial for achieving the considerable surface attributes for solvency as well as their favourable applications.

Due to the presence of different surface functionalities, these CQDs have been found to show different photo-luminescence behaviors. It has been observed that the different surface functional groups can interact with different sets of metal ions, and hence, the CQDs synthesized using different carbon sources can sense different metal ions. Thus, CQDs are the potential candidates for the detection of metal ions including environmental toxins such as mercury and lead. These chemosensors have showed low LOD values, which indicate their higher efficiencies. However, several challenges associated with CQDs are mainly their large-scale synthesis, isolation and purification. Several research groups are working near these lines for sustainable and viable use of CQDs.

Researchers are looking into a variety of carbon sources including agricultural by-products, biomass and food waste in order to establish environmentally friendly and low-cost routes to produce CQDs. These carbon sources are plentiful, renewable, and less expensive, which make them appealing alternatives to traditional sources. CQDs have the potential to be used in a variety of fields including bioimaging, optoelectronics and sensing. Undoubtedly, there will be challenges in improving the luminescence, quantum yield and electrochemical performance, and there is limited information on the mechanism of CQD synthesis, which researchers should consider further. In addition, the utilisation of green carbon sources for CQD synthesis is predicted to be beneficial for the development of sustainable technology.

Conflicts of interest

There are no conflicts to declare.

Acknowledgements

Authors acknowledge the support provided under the DST-FIST Grant No. SR/FST/PS-I/2018/48 of Government of India.

Notes and references

1 X. Wang, Y. Feng, P. Dong and J. Huang, *Front. Chem.*, 2019, **7**, 671–679.
2 A. Cayuela, M. L. Soriano, C. Carrillo-Carrión and M. Valcárcel, *Chem. Commun.*, 2016, **52**, 1311–1326.

3 X. Xu, R. Ray, Y. Gu, H. J. Ploehn, L. Gearheart, K. Raker and W. A. Scrivens, *J. Am. Chem. Soc.*, 2004, **126**, 12736–12737.
4 M. Semeniuk, Z. Yi, V. Poursorkhabi, J. Tjong, S. Jaffer, Z. H. Lu and M. Sain, *ACS Nano*, 2019, **13**, 6224–6255.
5 W. Su, H. Wu, H. Xu, Y. Zhang, Y. Li, X. Li and L. Fan, *Mater. Chem. Front.*, 2020, **4**, 821–836.
6 S. Mohapatra, S. Sahu, N. Sinha and S. K. Bhutia, *Analyst*, 2015, **140**, 1221–1228.
7 A. Rastogi, F. P. Pandey, A. S. Parmar, S. Singh, G. Hegde and R. Manohar, *J. Nanostruct. Chem.*, 2021, **11**, 527–548.
8 J. Scaria, A. V. Karim, G. Divyapriya, P. V. Nidheesh and M. Suresh Kumar, Carbon-supported semiconductor nanoparticles as effective photocatalysts for water and wastewater treatment, *Nano-Materials as Photocatalysts for Degradation of Environmental Pollutants: Challenges and Possibilities*, Elsevier Inc., 2020, pp. 245–278.
9 S. Qu, X. Wang, Q. Lu, X. Liu and L. Wang, *Angew. Chem., Int. Ed.*, 2012, **51**, 12215–12218.
10 F. Gao, Y. H. Zang, Y. Wang, C. Q. Guan, J. Y. Qu and M. B. Wu, *New Carbon Materials*, 2021, **36**, 34–48.
11 C. Tang, R. Long, X. Tong, Y. Guo, C. Tong and S. Shi, *Microchem. J.*, 2021, **164**, 106000.
12 B. De and N. Karak, *RSC Adv.*, 2013, **3**, 8286–8290.
13 D. Yoo, Y. Park, B. Cheon and M.-H. Park, *Nanoscale Res. Lett.*, 2019, **14**, 272.
14 S. Y. Lim, W. Shen and Z. Gao, *Chem. Soc. Rev.*, 2015, **44**, 362–381.
15 L. Han, D. Ghosh, W. Chen, S. Pradhan, X. Chang and S. Chen, *Chem. Mater.*, 2009, **21**, 2803–2809.
16 R. Liu, D. Wu, S. Liu, K. Koynov, W. Knoll and Q. Li, *Angew. Chem., Int. Ed.*, 2009, **48**, 4598–4601.
17 S. C. Ray, A. Saha, N. R. Jana and R. Sarkar, *J. Phys. Chem. C*, 2009, **113**, 18546–18551.
18 Z. A. Qiao, Y. Wang, Y. Gao, H. Li, T. Dai, Y. Liu and Q. Huo, *Chem. Commun.*, 2010, **46**, 8812–8814.
19 Y. P. Sun, B. Zhou, Y. Lin, W. Wang, K. A. S. Fernando, P. Pathak, M. J. Meziani, B. A. Harruff, X. Wang, H. Wang, P. G. Luo, H. Yang, M. E. Kose, B. Chen, L. M. Veca and S. Y. Xie, *J. Am. Chem. Soc.*, 2006, **128**, 7756–7757.
20 J. Deng, Q. Lu, N. Mi, H. Li, M. Liu, M. Xu, L. Tan, Q. Xie, Y. Zhang and S. Yao, *Chem.–Eur. J.*, 2014, **20**, 4993–4999.
21 S. Anwar, H. Ding, M. Xu, X. Hu, Z. Li, J. Wang, L. Liu, L. Jiang, D. Wang, C. Dong, M. Yan, Q. Wang and H. Bi, *ACS Appl. Bio Mater.*, 2019, **2**, 2317–2338.
22 M. Pan, X. Xie, K. Liu, J. Yang, L. Hong and S. Wang, *Nanomaterials*, 2020, **10**, 1–25.
23 H. Li, X. He, Y. Liu, H. Huang, S. Lian, S. T. Lee and Z. Kang, *Carbon*, 2011, **49**, 605–609.
24 H. Eskalen, S. Urus, S. Comertpay, A. H. Kurt and S. Ozgan, *Ind. Crops Prod.*, 2020, **147**, 112209.
25 C. B. Ma, Z. T. Zhu, H. X. Wang, X. Huang, X. Zhang, X. Qi, H. L. Zhang, Y. Zhu, X. Deng, Y. Peng, Y. Han and H. Zhang, *Nanoscale*, 2015, **7**, 10162–10169.
26 R. Atchudan, T. N. Jebakumar Immanuel Edison, M. Shanmugam, S. Perumal, T. Somanathan and Y. R. Lee, *Phys. E*, 2021, **126**, 114417.
27 J. Zong, Y. Zhu, X. Yang, J. Shen and C. Li, *Chem. Commun.*, 2011, **47**, 764–766.
28 X. Ma, S. Li, V. Hessel, L. Lin, S. Meskers and F. Gallucci, *Chem. Eng. Process.*, 2019, **140**, 29–35.
29 V. Thongpool, P. Asanithi and P. Limsuwan, *Procedia Eng.*, 2012, **32**, 1054–1060.
30 H. Zhu, X. Wang, Y. Li, Z. Wang, F. Yang and X. Yang, *Chem. Commun.*, 2009, 5118–5120.
31 W. Liu, C. Li, X. Sun, W. Pan, G. Yu and J. Wang, *Nanotechnology*, 2017, **28**, 18.
32 D. Gu, S. Shang, Q. Yu and J. Shen, *Appl. Surf. Sci.*, 2016, **390**, 38–42.
33 A. S. Kamarol Zaman, T. L. Tan, Y. A. P. Chowmasundaram, N. Jamaludin, A. R. Sadrolhosseini, U. Rashid and S. A. Rashid, *Opt. Mater.*, 2021, **112**, 110801.
34 N. R. Pires, C. M. W. Santos, R. R. Sousa, R. C. M. De Paula, P. L. R. Cunha and J. P. A. Feitosa, *J. Braz. Chem. Soc.*, 2015, **26**, 1274–1282.
35 S. S. Monte-filho, S. I. E. Andrade, M. B. Lima and M. C. U. Araujo, *J. Pharm. Anal.*, 2019, **9**, 209–216.
36 J. Bian, C. Huang, L. Wang, W. A. Daoud and R. Zhang, *ACS Appl. Mater. Interfaces*, 2014, **6**, 4883–4890.
37 S. Zhu, Q. Meng, L. Wang, J. Zhang, Y. Song, H. Jin, K. Zhang, H. Sun, H. Wang and B. Yang, *Angew. Chem.*, 2013, **52**, 3953–3957.
38 Z. M. S. H. Khan, R. S. Rahman, S. Shumaila, S. Islam and M. Zulfequar, *Opt. Mater.*, 2019, **91**, 386–395.
39 N. Arumugam and J. Kim, *Mater. Lett.*, 2018, **219**, 37–40.
40 W. Lu, X. Qin, S. Liu, G. Chang, Y. Zhang, Y. Luo, A. M. Asiri, A. O. Al-Youbi and X. Sun, *Anal. Chem.*, 2012, **84**, 5351–5357.
41 Y. Yang, J. Cui, M. Zheng, C. Hu, S. Tan, Y. Xiao, Q. Yang and Y. Liu, *Chem. Commun.*, 2012, **48**, 380–382.
42 C. Yu, D. Qin, X. Jiang, X. Zheng and B. Deng, *J. Pharm. Biomed. Anal.*, 2020, **192**, 113673.
43 P. K. Yadav, V. K. Singh, S. Chandra, D. Bano, V. Kumar, M. Talat and S. H. Hasan, *ACS Biomater. Sci. Eng.*, 2018, **5**, 623–632.
44 L. Zhang, Y. Wang, W. Liu, Y. Ni and Q. Hou, *Ind. Crops Prod.*, 2019, **133**, 18–25.
45 C. Cheng, Y. Shi, M. Li, M. Xing and Q. Wu, *Mater. Sci. Eng., C*, 2017, **79**, 473–480.
46 J. Zhou, Z. Sheng, H. Han, M. Zou and C. Li, *Mater. Lett.*, 2012, **66**, 222–224.
47 D. Sun, R. Ban, P. Zhang, G. Wu, J. Zhang and J. Zhu, *Carbon*, 2013, **64**, 424–434.
48 N. Murugan, M. Prakash, M. Jayakumar, A. Sundaramurthy and A. K. Sundramoorthy, *Appl. Surf. Sci.*, 2019, **476**, 468–480.
49 B. Yin, J. Deng, X. Peng, Q. Long, J. Zhao, Q. Lu, Q. Chen, H. Li, H. Tang, Y. Zhang and S. Yao, *Analyst*, 2013, **138**, 6551–6557.
50 R. Bandi, R. Dadigala, B. R. Gangapuram and V. Guttena, *J. Photochem. Photobiol., B*, 2018, **178**, 330–338.
51 M. J. Molaei, *Anal. Methods*, 2020, **12**, 1266–1287.
52 A. C. C. Esteves and T. Trindade, *Curr. Opin. Solid State Mater. Sci.*, 2002, **6**, 347–353.
53 L. Brus, *J. Phys. Chem.*, 1986, **90**, 2555–2560.

54 L. Qu and X. Peng, *J. Am. Chem. Soc.*, 2002, **124**, 2049–2055.
55 H. Li, X. He, Z. Kang, H. Huang, Y. Liu, J. Liu, S. Lian, C. H. A. Tsang, X. Yang and S. T. Lee, *Angew. Chem., Int. Ed.*, 2010, **49**, 4430–4434.
56 S. Sahu, B. Behera, T. K. Maiti and S. Mohapatra, *Chem. Commun.*, 2012, **48**, 8835–8837.
57 H. Ding, S. B. Yu, J. S. Wei and H. M. Xiong, *ACS Nano*, 2016, **10**, 484–491.
58 X. Deng, Y. Feng, H. Li, Z. Du, Q. Teng and H. Wang, *Particuology*, 2018, **41**, 94–100.
59 M. J. Krysmann, A. Kelarakis, P. Dallas and E. P. Giannelis, *J. Am. Chem. Soc.*, 2012, **134**, 747–750.
60 X. Wen, P. Yu, Y. R. Toh, X. Ma and J. Tang, *Chem. Commun.*, 2014, **50**, 4703–4706.
61 C. S. Stan, C. Albu, A. Coroaba, M. Popa and D. Sutiman, *J. Mater. Chem. C*, 2015, **3**, 789–795.
62 K. Jiang, S. Sun, L. Zhang, Y. Lu, A. Wu, C. Cai and H. Lin, *Angew. Chem., Int. Ed.*, 2015, **54**, 5360–5363.
63 X. Gao, C. Du, Z. Zhuang and W. Chen, *J. Mater. Chem. C*, 2016, **4**, 6927–6945.
64 H. Feng and Z. Qian, *Chem. Rec.*, 2018, **18**, 491–505.
65 X. Wang, L. Cao, S. T. Yang, F. Lu, M. J. Meziani, L. Tian, K. W. Sun, M. A. Bloodgood and Y. P. Sun, *Angew. Chem.*, 2010, **49**, 5310–5314.
66 M. J. Molaei, *Talanta*, 2019, **196**, 456–478.
67 J. Liao, Z. Cheng and L. Zhou, *ACS Sustain. Chem. Eng.*, 2016, **4**, 3053–3061.
68 V. Ramanan, B. Siddaiah, K. Raji and P. Ramamurthy, *ACS Sustain. Chem. Eng.*, 2018, **6**, 1627–1638.
69 X. W. Tan, A. N. B. Romainor, S. F. Chin and S. M. Ng, *J. Anal. Appl. Pyrolysis*, 2014, **105**, 157–165.
70 S. Ravi and M. K. Jayaraj, *Emergent Mater.*, 2020, **3**, 51–56.
71 J. Bi, H. Wang, T. Kamal, B. W. Zhu and M. Tan, *RSC Adv.*, 2017, **7**, 30481–30487.
72 L. Wang, B. Li, F. Xu, X. Shi, D. Feng, D. Wei, Y. Li, Y. Feng, Y. Wang, D. Jia and Y. Zhou, *Biosens. Bioelectron.*, 2016, **79**, 1–8.
73 A. Sachdev and P. Gopinath, *Analyst*, 2015, **140**, 4260–4269.
74 Y. Liu, Y. Zhao and Y. Zhang, *Sens. Actuators, B*, 2014, **196**, 647–652.
75 P. Krishnaiah, R. Atchudan, S. Perumal, E. S. Salama, Y. R. Lee and B. H. Jeon, *Chemosphere*, 2022, **286**, 131764–131773.
76 T. D. Gauthier, E. C. Shane, W. F. Guerin, W. R. Seitz and C. L. Grant, *Environ. Sci. Technol.*, 1986, **20**, 1162–1166.
77 F. Zu, F. Yan, Z. Bai, J. Xu, Y. Wang, Y. Huang and X. Zhou, *Microchim. Acta*, 2017, **184**, 1899–1914.
78 M. Zheng, Z. Xie, D. Qu, D. Li, P. Du, X. Jing and Z. Sun, *ACS Appl. Mater. Interfaces*, 2013, **5**, 13242–13247.
79 D. A. Gupta, M. L. Desai, N. I. Malek and S. K. Kailasa, *J. Mol. Struct.*, 2020, **1216**, 128343.
80 P. Devi, P. Rajput, A. Thakur, K. H. Kim and P. Kumar, *TrAC, Trends Anal. Chem.*, 2019, **114**, 171–195.
81 Z. Liang, M. Kang, G. F. Payne, X. Wang and R. Sun, *ACS Appl. Mater. Interfaces*, 2016, **8**, 17478–17488.
82 H. Liu, C. Xu, Y. Bai, L. Liu, D. Liao, J. Liang, L. Liu and H. Han, *Spectrochim. Acta, Part A*, 2017, **171**, 311–316.
83 G. B. Kim and Y. P. Kim, *Theranostics*, 2012, **2**, 127–138.
84 J. Shen, S. Shang, X. Chen, D. Wang and Y. Cai, *Mater. Sci. Eng., C*, 2017, **76**, 856–864.
85 Y. Chen and Z. Rosenzweig, *Anal. Chem.*, 2002, **74**, 5132–5138.
86 M. C. Rong, K. X. Zhang, Y. R. Wang and X. Chen, *Chin. Chem. Lett.*, 2017, **28**, 1119–1124.
87 Y. Ru, G. I. N. Waterhouse and S. Lu, *Aggregate*, 2022, 1–14.
88 V. A. Ansi and N. K. Renuka, *Sens. Actuators, B*, 2018, **264**, 67–75.
89 K. Raji, V. Ramanan and P. Ramamurthy, *New J. Chem.*, 2019, **43**, 11710–11719.
90 X. Sun and Y. Lei, *TrAC, Trends Anal. Chem.*, 2017, **89**, 163–180.
91 J. R. Lakowicz, *Princ. Fluoresc. Spectrosc.*, 1983, 303–339.
92 Y. Z. Fan, Y. Zhang, N. Li, S. G. Liu, T. Liu, N. B. Li and H. Q. Luo, *Sens. Actuators, B*, 2017, **240**, 949–955.
93 C. Liu, B. Tang, S. Zhang, M. Zhou, M. Yang, Y. Liu, Z. L. Zhang, B. Zhang and D. W. Pang, *J. Phys. Chem. C*, 2018, **122**, 3662–3668.
94 Y. Song, S. Zhu, S. Xiang, X. Zhao, J. Zhang, H. Zhang, Y. Fu and B. Yang, *Nanoscale*, 2014, **6**, 4676–4682.
95 K. Chen, W. Qing, W. Hu, M. Lu, Y. Wang and X. Liu, *Spectrochim. Acta, Part A*, 2019, **213**, 228–234.
96 S. A. A. Vandarkuzhali, S. Natarajan, S. Jeyabalan, G. Sivaraman, S. Singaravadivel, S. Muthusubramanian and B. Viswanathan, *ACS Omega*, 2018, **3**, 12584–12592.
97 Y. Liu, Q. Zhou, J. Li, M. Lei and X. Yan, *Sens. Actuators, B*, 2016, **237**, 597–604.
98 R. Purbia and S. Paria, *Biosens. Bioelectron.*, 2016, **79**, 467–475.
99 Y. Sha, J. Lou, S. Bai, D. Wu, B. Liu and Y. Ling, *Mater. Res. Bull.*, 2013, **48**, 1728–1731.
100 Y. Lou, Y. Zhao, J. Chen and J. J. Zhu, *J. Mater. Chem. C*, 2014, **2**, 595–613.
101 A. Shander, M. D. Cappellini and L. T. Goodnough, *Vox Sang.*, 2009, **97**, 185–197.
102 R. Atchudan, T. N. J. I. Edison, D. Chakradhar, S. Perumal, J. J. Shim and Y. R. Lee, *Sens. Actuators, B*, 2017, **246**, 497–509.
103 N. Architha, M. Ragupathi, C. Shobana, T. Selvankumar, P. Kumar, Y. S. Lee and R. Kalai Selvan, *Environ. Res.*, 2021, **199**, 111263–111273.
104 H. Ma, C. Sun, G. Xue, G. Wu, X. Zhang, X. Han, X. Qi, X. Lv, H. Sun and J. Zhang, *Spectrochim. Acta, Part A*, 2019, **213**, 281–287.
105 F. Wu, M. Yang, H. Zhang, S. Zhu, X. Zhu and K. Wang, *Opt. Mater.*, 2018, **77**, 258–263.
106 A. M. Aslandaş, N. Balci, M. Arik, H. Şakiroğlu, Y. Onganer and K. Meral, *Appl. Surf. Sci.*, 2015, **356**, 747–752.
107 M. Lu, Y. Duan, Y. Song, J. Tan and L. Zhou, *J. Mol. Liq.*, 2018, **269**, 766–774.
108 W. Liu, H. Diao, H. Chang, H. Wang, T. Li and W. Wei, *Sens. Actuators, B*, 2017, **241**, 190–198.
109 R. Yang, X. Guo, L. Jia, Y. Zhang, Z. Zhao and F. Lonshakov, *Appl. Surf. Sci.*, 2017, **423**, 426–432.

110 G. Venkatesan, V. Rajagopalan and S. N. Chakravarthula, *J. Environ. Chem. Eng.*, 2019, **7**, 103013.
111 K. J. Barnham and A. I. Bush, *Chem. Soc. Rev.*, 2014, **43**, 6727–6749.
112 N. Chaudhary, P. K. Gupta, S. Eremin and P. R. Solanki, *J. Environ. Chem. Eng.*, 2020, **8**, 103720.
113 J. Y. Tai, K. H. Leong, P. Saravanan, S. T. Tan, W. C. Chong and L. C. Sim, *J. Environ. Chem. Eng.*, 2020, **9**, 104622.
114 Q. Qu, A. Zhu, X. Shao and Y. Tian, *Chem. Commun.*, 2012, **48**, 5473–5475.
115 G. Gedda, C. Y. Lee, Y. C. Lin and H. F. Wu, *Sens. Actuators, B*, 2016, **224**, 396–403.
116 K. Bera, A. K. Das, M. Nag and S. Basak, *Anal. Chem.*, 2014, **86**, 2740–2746.
117 L. D. Hylander and M. E. Goodsite, *Sci. Total Environ.*, 2006, **368**, 352–370.
118 X. Qin, W. Lu, A. M. Asiri, A. O. Al-Youbi and X. Sun, *Sens. Actuators, B*, 2013, **184**, 156–162.
119 Y. Xie, D. Cheng, X. Liu and A. Han, *Sensors*, 2019, **19**, 3169.
120 L. S. Li, X. Y. Jiao, Y. Zhang, C. Cheng, K. Huang and L. Xu, *Sens. Actuators, B*, 2018, **263**, 426–435.
121 D. Bano, V. Kumar, V. K. Singh and S. H. Hasan, *New J. Chem.*, 2018, **42**, 5814–5821.
122 A. Gupta, N. C. Verma, S. Khan, S. Tiwari, A. Chaudhary and C. K. Nandi, *Sens. Actuators, B*, 2016, **232**, 107–114.
123 A. Kumar, A. R. Chowdhuri, D. Laha, T. K. Mahto, P. Karmakar and S. K. Sahu, *Sens. Actuators, B*, 2017, **242**, 679–686.
124 Z. Liu, W. Jin, F. Wang, T. Li, J. Nie, W. Xiao, Q. Zhang and Y. Zhang, *Sens. Actuators, B*, 2019, **296**, 126698.
125 A. Tyagi, K. M. Tripathi, N. Singh, S. Choudhary and R. K. Gupta, *RSC Adv.*, 2016, **6**, 72423–72432.
126 Z. Ramezani, M. Qorbanpour and N. Rahbar, *Colloids Surf., A*, 2018, **549**, 58–66.
127 K. Radhakrishnan and P. Panneerselvam, *RSC Adv.*, 2018, **8**, 30455–30467.
128 A. Dutta, B. Rooj, T. Mondal, D. Mukherjee and U. Mandal, *J. Iran. Chem. Soc.*, 2020, **17**, 1695–1704.
129 C. Zhao, X. Li, C. Cheng and Y. Yang, *Microchem. J.*, 2019, **147**, 183–190.
130 J. R. Bhamore, S. Jha, R. K. Singhal, T. J. Park and S. K. Kailasa, *J. Mol. Liq.*, 2018, **264**, 9–16.
131 X. Yang, Y. Zhuo, S. Zhu, Y. Luo, Y. Feng and Y. Dou, *Biosens. Bioelectron.*, 2014, **60**, 292–298.
132 S. A. A. Vandarkuzhali, V. Jeyalakshmi, G. Sivaraman, S. Singaravadivel, K. R. Krishnamurthy and B. Viswanathan, *Sens. Actuators, B*, 2017, **252**, 894–900.
133 G. Huang, X. Chen, C. Wang, H. Zheng, Z. Huang, D. Chen and H. Xie, *RSC Adv.*, 2017, **7**, 47840–47847.
134 R. Bandi, B. R. Gangapuram, R. Dadigala, R. Eslavath, S. S. Singh and V. Guttena, *RSC Adv.*, 2016, **6**, 28633–28639.
135 W. Zhang, L. Jia, X. Guo, R. Yang, Y. Zhang and Z. Zhao, *Analyst*, 2019, **144**, 7421–7431.
136 S. K. Kailasa, S. Ha, S. H. Baek, L. M. T. Phan, S. Kim, K. Kwak and T. J. Park, *Mater. Sci. Eng., C*, 2019, **98**, 834–842.
137 W. B. Zhao, K. K. Liu, S. Y. Song, R. Zhou and C. X. Shan, *Nanoscale Res. Lett.*, 2019, **14**, 130.
138 J. Singh, S. Kaur, J. Lee, A. Mehta, S. Kumar, K. H. Kim, S. Basu and M. Rawat, *Sci. Total Environ.*, 2020, **720**, 137604.
139 M. Das, H. Thakkar, D. Patel and S. Thakore, *J. Environ. Chem. Eng.*, 2021, **9**, 106312.
140 S. Raja, E. M. Buhl, S. Dreschers, C. Schalla, M. Zenke, A. Sechi and L. H. C. Mattoso, *Mater. Sci. Eng., C*, 2021, **129**, 112409.
141 X. Sun, J. He, S. Yang, M. Zheng, Y. Wang, S. Ma and H. Zheng, *J. Photochem. Photobiol., B*, 2017, **175**, 219–225.
142 R. Atchudan, T. N. J. I. Edison, S. Perumal, N. Muthuchamy and Y. R. Lee, *Fuel*, 2020, **275**, 117821.
143 H. Liu, Y. Zhang, J. H. Liu, P. Hou, J. Zhou and C. Z. Huang, *RSC Adv.*, 2017, **7**, 50584–50590.
144 H. Diao, T. Li, R. Zhang, Y. Kang, W. Liu, Y. Cui, S. Wei, N. Wang, L. Li, H. Wang, W. Niu and T. Sun, *Spectrochim. Acta, Part A*, 2018, **200**, 226–234.
145 H. Qi, M. Teng, M. Liu, S. Liu, J. Li, H. Yu, C. Teng, Z. Huang, H. Liu, Q. Shao, A. Umar, T. Ding, Q. Gao and Z. Guo, *J. Colloid Interface Sci.*, 2019, **539**, 332–341.
146 T. K. Mondal, A. Gupta, B. K. Shaw, S. Mondal, U. K. Ghorai and S. K. Saha, *RSC Adv.*, 2016, **6**, 59927–59934.
147 R. Atchudan, T. N. J. I. Edison, S. Perumal, R. Vinodh, A. K. Sundramoorthy, R. S. Babu and Y. R. Lee, *Chemosensors*, 2021, **9**, 1–15.
148 R. Atchudan, T. N. J. I. Edison, S. Perumal, R. Vinodh and Y. R. Lee, *J. Mol. Liq.*, 2019, **296**, 111817.
149 T. N. J. I. Edison, R. Atchudan, J. J. Shim, S. Kalimuthu, B. C. Ahn and Y. R. Lee, *J. Photochem. Photobiol., B*, 2016, **158**, 235–242.
150 R. Atchudan, T. N. J. I. Edison, K. R. Aseer, S. Perumal and Y. R. Lee, *Colloids Surf., B*, 2018, **169**, 321–328.
151 M. Preethi, C. Viswanathan and N. Ponpandian, *Particuology*, 2021, **58**, 251–258.
152 S. Zhao, X. Song, X. Chai, P. Zhao, H. He and Z. Liu, *J. Cleaner Prod.*, 2020, **263**, 121561.
153 N. K. Sahoo, G. C. Jana, M. N. Aktara, S. Das, S. Nayim, A. Patra, P. Bhattacharjee, K. Bhadra and M. Hossain, *Mater. Sci. Eng., C*, 2020, **108**, 110429.
154 K. Kalanidhi and P. Nagaraaj, *J. Photochem. Photobiol., A*, 2021, **418**, 113369.
155 N. Wang, Y. Wang, T. Guo, T. Yang, M. Chen and J. Wang, *Biosens. Bioelectron.*, 2016, **85**, 68–75.
156 A. T. Nkeumaleu, D. Benetti, I. Haddadou, M. Di Mare, C. M. Ouellet-Plamondon and F. Rosei, *RSC Adv.*, 2022, **12**, 11621–11627.
157 M. Zulfajri, G. Gedda, C. J. Chang, Y. P. Chang and G. G. Huang, *ACS Omega*, 2019, **4**, 15382–15392.
158 T. Arumugham, M. Alagumuthu, R. G. Amimodu, S. Munusamy and S. K. Iyer, *Sustainable Mater. Technol.*, 2020, **23**, e00138.
159 J. Ahn, Y. Song, J. E. Kwon, J. Woo and H. Kim, *Data Brief*, 2019, **25**, 104038.
160 X. Y. Jiao, L. shuang Li, S. Qin, Y. Zhang, K. Huang and L. Xu, *Colloids Surf., A*, 2019, **577**, 306–314.

161 S. Venkatesan, A. J. Mariadoss, A. Kathiravan and A. Muthupandian, *Sens. Actuators, B*, 2019, **282**, 972–983.
162 P. Das, S. Ganguly, P. P. Maity, M. Bose, S. Mondal, S. Dhara, A. K. Das, S. Banerjee and N. C. Das, *J. Photochem. Photobiol., B*, 2018, **180**, 56–67.
163 P. Song, L. Zhang, H. Long, M. Meng, T. Liu, Y. Yin and R. Xi, *RSC Adv.*, 2017, **7**, 28637–28646.
164 R. Liu, J. Zhang, M. Gao, Z. Li, J. Chen, D. Wu and P. Liu, *RSC Adv.*, 2015, **5**, 4428–4433.
165 L. Liu, S. Zhang, X. Zheng, H. Li, Q. Chen, K. Qin, Y. Ding and Y. Wei, *Anal. Methods*, 2021, **13**, 1121–1131.
166 J. Zhao, M. Huang, L. Zhang, M. Zou, D. Chen, Y. Huang and S. Zhao, *Anal. Chem.*, 2017, **89**, 8044–8049.
167 N. Pourreza and M. Ghomi, *Mater. Sci. Eng., C*, 2019, **98**, 887–896.
168 H. Huang, J. J. Lv, D. L. Zhou, N. Bao, Y. Xu, A. J. Wang and J. J. Feng, *RSC Adv.*, 2013, **3**, 21691–21696.
169 G. Liu, H. Jia, N. Li, X. Li, Z. Yu, J. Wang and Y. Song, *Microchem. J.*, 2019, **145**, 718–728.
170 K. Srinivasan, K. Subramanian, K. Murugan and K. Dinakaran, *Analyst*, 2016, **141**, 6344–6352.
171 J. Yu, N. Song, Y. K. Zhang, S. X. Zhong, A. J. Wang and J. Chen, *Sens. Actuators, B*, 2015, **214**, 29–35.
172 V. Roshni and D. Ottoor, *J. Lumin.*, 2015, **161**, 117–122.
173 C. Wang, D. Sun, K. Zhuo, H. Zhang and J. Wang, *RSC Adv.*, 2014, **4**, 54060–54065.
174 M. L. Desai, S. Jha, H. Basu, R. K. Singhal, T. J. Park and S. K. Kailasa, *ACS Omega*, 2019, **4**, 19332–19340.
175 A. K. Singh, V. K. Singh, M. Singh, P. Singh, S. R. Khadim, U. Singh, B. Koch, S. H. Hasan and R. K. Asthana, *J. Photochem. Photobiol., A*, 2019, **376**, 63–72.
176 Z. Li, Y. Ni and S. Kokot, *Biosens. Bioelectron.*, 2015, **74**, 91–97.
177 P. M. Gharat, H. Pal and S. Dutta Choudhury, *Spectrochim. Acta, Part A*, 2019, **209**, 14–21.
178 J. Wei, X. Zhang, Y. Sheng, J. Shen, P. Huang, S. Guo, J. Pan and B. Feng, *Mater. Lett.*, 2014, **123**, 107–111.
179 J. B. Essner, C. H. Laber, S. Ravula, L. Polo-Parada and G. A. Baker, *Green Chem.*, 2016, **18**, 243–250.
180 X. Ma, Y. Dong, H. Sun and N. Chen, *Mater. Today Chem.*, 2017, **5**, 1–10.
181 P. Das, S. Ganguly, M. Bose, S. Mondal, A. K. Das, S. Banerjee and N. C. Das, *Mater. Sci. Eng., C*, 2017, **75**, 1456–1464.
182 X. Zhu, H. Jin, C. Gao, R. Gui and Z. Wang, *Talanta*, 2017, **162**, 65–71.
183 S. Liu, J. Tian, L. Wang, Y. Zhang, X. Qin, Y. Luo, A. M. Asiri, A. O. Al-Youbi and X. Sun, *Adv. Mater.*, 2012, **24**, 2037–2041.
184 W. Zhang, N. Li, Q. Chang, Z. Chen and S. Hu, *Colloids Surf., A*, 2020, **586**, 124233.
185 Y. Wang, W. T. Wu, M. B. Wu, H. Di Sun, H. Xie, C. Hu, X. Y. Wu and J. S. Qiu, *New Carbon Materials*, 2015, **30**, 550–559.
186 P. Shasha, J. H. Kim and S. J. Park, *J. Nanosci. Nanotechnol.*, 2019, **19**, 6077–6082.
187 L. Liu, H. Gong, D. Li and L. Zhao, *J. Nanosci. Nanotechnol.*, 2018, **18**, 5327–5332.
188 S. Sharma, A. Umar, S. K. Mehta and S. K. Kansal, *Ceram. Int.*, 2017, **43**, 7011–7019.
189 P. Devi, L. Singh, A. Thakur and P. Kumar, *Sens. Actuators, B*, 2019, **283**, 363–372.
190 S. Bhatt, M. Bhatt, A. Kumar, G. Vyas, T. Gajaria and P. Paul, *Colloids Surf., B*, 2018, **167**, 126–133.
191 S. Feng, Z. Gao, H. Liu, J. Huang, X. Li and Y. Yang, *Spectrochim. Acta, Part A*, 2019, **212**, 286–292.
192 M. Athika, A. Prasath, E. Duraisamy, V. Sankar Devi, A. Selva Sharma and P. Elumalai, *Mater. Lett.*, 2019, **241**, 156–159.
193 K. M. Tripathi, A. Singh, A. Bhati, S. Sarkar and S. K. Sonkar, *ACS Sustain. Chem. Eng.*, 2016, **4**, 6399–6408.
194 V. Roshni, S. Misra, M. K. Santra and D. Ottoor, *J. Photochem. Photobiol., A*, 2019, **373**, 28–36.
195 S. Chaudhary, S. Kumar, B. Kaur and S. K. Mehta, *RSC Adv.*, 2016, **6**, 90526–90536.
196 S. Jing, Y. Zhao, R. C. Sun, L. Zhong and X. Peng, *ACS Sustain. Chem. Eng.*, 2019, **7**, 7833–7843.
197 J. Xu, X. Jie, F. Xie, H. Yang, W. Wei and Z. Xia, *Nano Res.*, 2018, **11**, 3648–3657.
198 Z. Dongqiang, Y. Wang, J. Xu, H. Li, M. Du, X. Liu and K. Wang, *Am. Sci. Publ.*, 2020, **10**, 596–601.
199 F. Akhgari, K. Farhadi, N. Samadi and M. Akhgari, *Iran. J. Sci. Technol., Trans. A: Sci.*, 2020, **44**, 379–387.
200 A. Suryawanshi, M. Biswal, D. Mhamane, R. Gokhale, S. Patil, D. Guin and S. Ogale, *Nanoscale*, 2014, **6**, 11664–11670.
201 Z. Rahmani and M. Ghaemy, *Opt. Mater.*, 2019, **97**, 109356.
202 J. R. Bhamore, T. J. Park and S. K. Kailasa, *J. Anal. Sci. Technol.*, 2020, **11**, 13.
203 S. Jayaweera, K. Yin, X. Hu and W. J. Ng, *J. Fluoresc.*, 2019, **29**, 1291–1300.
204 C. Yu, D. Qin, X. Jiang, X. Zheng and B. Deng, *J. Pharm. Biomed. Anal.*, 2021, **192**, 113673.
205 R. Qiang, S. Yang, K. Hou and J. Wang, *New J. Chem.*, 2019, **43**, 10826–10833.
206 D. Ghosh Dastidar, P. Mukherjee, D. Ghosh and D. Banerjee, *Colloids Surf., A*, 2020, **611**, 125781.
207 P. Devi, G. Kaur, A. Thakur, N. Kaur, A. Grewal and P. Kumar, *Talanta*, 2017, **170**, 49–55.
208 B. T. Hoan, T. T. Thanh, P. D. Tam, N. N. Trung, S. Cho and V. H. Pham, *Mater. Sci. Eng., B*, 2019, **251**, 114455.
209 A. Başoğlu, Ü. Ocak and A. Gümrükçüoğlu, *J. Fluoresc.*, 2020, **30**, 515–526.
210 U. Latief, S. ul Islam, Z. M. S. H. Khan and M. S. Khan, *Spectrochim. Acta, Part A*, 2021, **262**, 120132.
211 N. H. Zainal Abidin, V. Wongso, K. C. Hui, K. Cho, N. S. Sambudi, W. L. Ang and B. Saad, *J. Water Process. Eng.*, 2020, **38**, 101634.
212 H. Singh, A. Bamrah, M. Khatri and N. Bhardwaj, *Mater. Today: Proc.*, 2020, **28**, 1891–1894.
213 Z. Ye, Y. Zhang, G. Li and B. Li, *Anal. Lett.*, 2020, **53**, 2841–2853.
214 T. Boobalan, M. Sethupathi, N. Sengottuvelan, P. Kumar, P. Balaji, B. Gulyás, P. Padmanabhan, S. T. Selvan and A. Arun, *ACS Appl. Nano Mater.*, 2020, **3**, 5910–5919.

215 A. M. Senol and E. Bozkurt, *Microchem. J.*, 2020, **159**, 105357.
216 D. Tai, C. Liu and J. Liu, *Spectrosc. Lett.*, 2019, **52**, 194–199.
217 B. Luo, H. Yang, B. Zhou, S. M. Ahmed, Y. Zhang, H. Liu, X. Liu, Y. He and S. Xia, *ACS Omega*, 2020, **5**, 5540–5547.
218 S. C. Pandey, A. Kumar and S. K. Sahu, *J. Photochem. Photobiol., A*, 2020, 112620.
219 P. Murugesan, J. A. Moses and C. Anandharamakrishnan, *Spectrosc. Lett.*, 2020, 1–9.
220 C. Wang, J. Xu, H. Li and W. Zhao, *Luminescence*, 2020, **35**, 1373–1383.
221 W. X. Yan and W. T. Qi, *Surf. Interface Anal.*, 2019, **52**, 1–8.
222 N. Hashemi and M. H. Mousazadeh, *J. Photochem. Photobiol., A*, 2021, **421**, 113534.
223 M. Carolina, R. Vieira, F. Andrade, M. Krambeck, D. O. Franco, W. Toito, C. Bandane, M. Henrique and F. F. Gambarra-neto, *Ecotoxicol. Environ. Saf.*, 2021, **213**, 112043.
224 B. Polatoğlu and E. Bozkurt, *Res. Chem. Intermed.*, 2021, **47**, 1865–1881.
225 L. D. Kasmiarno, A. Fikarda and R. K. Gunawan, *Waste Technol.*, 2021, **9**, 1–10.
226 G. Hu, L. Ge, Y. Li, M. Mukhtar, B. Shen and D. Yang, *J. Colloid Interface Sci.*, 2020, **579**, 96–108.
227 P. Sagar, K. Gupta and M. Srivastava, *RCS Adv.*, 2021, **11**, 19924–19934.
228 M. Zulfajri, K. Liu, Y. Pu, A. Rasool and S. Dayalan, *Chemosensors*, 2020, **8**, 47.
229 C. Zhou, S. Wu, S. Qi, W. Song and C. Sun, *J. Anal. Methods Chem.*, 2021, **2021**, 9732364.
230 D. Raja and D. Sundaramurthy, *Mater. Today: Proc.*, 2018, **34**, 488–492.
231 J. Li, O. Xu and X. Zhu, *RSC Adv.*, 2021, **11**, 34107–34116.
232 G. Chellasamy, S. K. Arumugasamy, S. Govindaraju and K. Yun, *Chemosphere*, 2022, **287**, 131915.
233 K. Kasinathan, S. Samayanan, K. Marimuthu and J. Yim, *Appl. Surf. Sci.*, 2022, **601**, 154266.
234 M. Nagaraj, S. Ramalingam, C. Murugan, S. Aldawood, J. O. Jin, I. Choi and M. Kim, *Environ. Res.*, 2022, **212**, 113273.
235 L. Gu, J. Zhang, G. Yang, Y. Tang, X. Zhang, X. Huang, W. Zhai, E. Kouadio and C. Kong, *Food Chem.*, 2022, **376**, 131898.
236 Y. Song, N. Qi, K. Li, D. Cheng, D. Wang and Y. Li, *RSC Adv.*, 2022, **12**, 8108–8118.
237 P. Zhao, Q. Zhang, J. Cao, C. Qian, J. Ye, S. Xu, Y. Zhang and Y. Li, *Nanomaterials*, 2022, **12**, 1528.
238 M. Sivanandhan, A. Parasuraman, C. Surya, K. Lakshminarayanan, B. Krishnakumar, D. Mani and Y. H. Ahn, *Inorg. Chem. Commun.*, 2022, **137**, 109219.
239 D. Elango, J. Saranya Packialakshmi, V. Manikandan and P. Jayanthi, *Mater. Lett.*, 2022, **313**, 131822.
240 Y. Qiu, D. Li, Y. Li, X. Ma and J. Li, *Cellulose*, 2022, **29**, 367–378.
241 Q. Huang, Q. Bao, C. Wu, M. Hu, Y. Chen, L. Wang and W. Chen, *J. Pharm. Anal.*, 2022, **12**, 104–112.
242 L. He, W. Pan, W. Qian, H. Wang, X. Hu and S. Chen, *Soc. Sci. Res.*, 2022, 1–24.
243 J. Yang, Z. Guo and X. Yue, *BioResources*, 2022, 604–615.
244 G. Ashok Varman, K. Kalanidhi and P. Nagaraaj, *Dyes Pigm.*, 2022, **199**, 110101.
245 D. Nugroho, W. Oh, S. Chanthai and R. Benchawattananon, *Res. Sq.*, 2023, DOI: **10.21203/rs.3.rs-1801504/v1.License**.
246 J. Mejía Ávila, M. Rangel Ayala, Y. Kumar, E. Pérez-Tijerina, M. A. R. Robles and V. Agarwal, *Chem. Eng. J.*, 2022, **446**, 1–12.
247 G. Ge, L. Li, M. Chen, X. Wu, Y. Yang, D. Wang, S. Zuo, Z. Zeng, W. Xiong and C. Guo, *Nanomaterials*, 2023, **12**, 986–998.
248 R. Atchudan, T. N. J. I. Edison, S. Perumal, R. Vinodh, A. K. Sundramoorthy, R. S. Babu and Y. R. Lee, *Colloids Surf., A*, 2022, **635**, 1–11.
249 S. Wang, X. Huo, H. Zhao, Y. Dong, Q. Cheng and Y. Li, *Chem. Phys. Impact*, 2022, **5**, 100112.
250 S. Tang, D. Chen, G. Guo, X. Li, C. Wang, T. Li and G. Wang, *Sci. Total Environ.*, 2022, **825**, 153913.
251 H. Khalid, M. F. Khan, B. Ahmad, M. Ismail, M. Zahid and A. Ismail, *J. Mater. Sci.: Mater. Electron.*, 2022, **33**, 5626–5634.
252 R. Fan, J. Xiang, P. Zhou, H. Mei, Y. Li, H. Wang, X. Liu and X. Wang, *Ecotoxicol. Environ. Saf.*, 2022, **15**, 113350.
253 C Zhang, X. Zheng, Y. Bai, Q. Luo, J. Shang, L. Xie and Y. Wei, *Nano*, 2022, **17**, 225003–225011.
254 B. K. Korah, M. S. Punnoose, C. R. Thara, T. Abraham, K. G. Ambady and B. Mathew, *Diamond Relat. Mater.*, 2022, **125**, 108980.
255 A. Sekar, R. Yadav and D. Easwaramoorthy, *Mater. Today: Proc.*, 2019, **48**, 427–437.
256 K. Raji, S. K. Thiyagarajan, R. Suresh, R. Vadivel, D. Palanivel and P. Ramamurthy, *Colloids Surf., A*, 2022, **641**, 128523.
257 W. Zhang, L. Hao, L. Shang, D. F. Chai, Y. Gao, J. Li, M. Zhao, R. Liu, Z. Zhang and G. Dong, *Nanotechnology*, 2022, **33**, 275707.
258 D. Mohapatra, R. Pratap, V. Pandey, P. Dubey, A. Agrawal, A. Parmar and A. Sahu, *J. Fluoresc.*, 2022, **32**, 275–292.
259 N. K. Quang and L. V. T. Son, *MRS Adv.*, 2022, **7**, 278–283.
260 J. Shi, Y. Zhou, J. Ning, G. Hu, Q. Zhang, Y. Hou and Y. Zhou, *Spectrochim. Acta, Part A*, 2022, **281**, 121597.
261 K. Phetcharee, N. Sirisit, P. Amonpattaratkit, J. Manyam and P. Paoprasert, *ChemistrySelect*, 2022, **7**, e202201280.
262 J. Zhang, G. Zheng, Y. Tian, C. Zhang, Y. Wang, M. Liu, D. Ren, H. Sun and W. Yu, *Inorg. Chem. Commun.*, 2022, **144**, 109837.
263 A. Tony Elizabeth, E. James, L. Infant Jesan, S. Denis Arockiaraj and A. Edwin Vasu, *Inorg. Chem. Commun.*, 2023, **149**, 110427.
264 Sariga, M. K. A. Kolaprath, L. Benny and A. Varghese, *Dyes Pigm.*, 2023, **210**, 111048.
265 B. K. Korah and B. Mathew, *Mater. Today Sustain.*, 2023, **21**, 100273.
266 G. Jeong, C. H. Park, D. Yi and H. Yang, *J. Cleaner Prod.*, 2023, **392**, 136250.

267 R. Atchudan, S. Perumal, T. N. J. I. Edison, A. K. Sundramoorthy, R. Vinodh, S. Sangaraju, S. C. Kishore and Y. R. Lee, *Sensors*, 2023, **23**, 787.
268 B. K. John, N. John and B. Mathew, *Mater. Today: Proc.*, 2023, **72**, 169–174.
269 B. Wang, L. Guo, X. Yan, F. Hou, L. Zhong and H. Xu, *Spectrochim. Acta, Part A*, 2023, **285**, 121891.
270 L. Zhang, B. Li, Y. Zhou, Y. Wu, T. Le and Q. Sun, *J. Sol-Gel Sci. Technol.*, 2023, **106**, 173–185.
271 S. Bhatt, G. Vyas and P. Paul, *Anal. Methods*, 2022, **14**, 269–277.
272 A. M. Babu, G. Bijoy, P. Keerthana and A. Varghese, *Synth. Met.*, 2022, **291**, 117211.